University of Alberta

Ice-Atmosphere Interactions on the Devon Ice Cap, Canada: the Effects of Climate Warming on Surface Energy Balance, Melting, and Firn Stratigraphy

by

Gabrielle Gascon

A thesis submitted to the Faculty of Graduate Studies and Research
in partial fulfillment of the requirements for the degree of

Doctor of Philosophy

Earth and Atmospheric Sciences

Spring 2014
Edmonton, Alberta

À ma grand-mère, Gigi. Tout a commencé en écoutant le réfrigérateur, classant des roches, et regardant les nuages avec toi. Après plusieurs années d'effort, j'ai enfin eu mon doctorat!

*****

To my grandmother, Gigi. It all started with listening to the refrigerator, and looking at rocks and clouds with you. After many years of hard work, I finally got a doctorate!

Abstract

In order to better constrain the magnitude of projected sea-level rise from Canadian Arctic glaciers during the 21st century warming, it is critical to understand the environmental mechanisms that enhance surface warming and melt, and how the projected increase in surface melt will translate into increased runoff. Between 2004 and 2010, a 4 °C increase in mean air summer temperature, and a 6.1 day yr^{-1} increase in melt season duration were observed on the Devon Ice Cap, Nunavut. At the same time, a combination of strengthening of the 500 hPa ridge over the Arctic in June-July, and more frequent south-westerly low-pressure systems in August after 2005 created atmospheric conditions that contributed to an increase in the surface energy balance of the ice cap. At 1400m elevation, these changes led to a doubling of the available melt energy and surface melt between 2007 and 2010. Over that same time period, increased meltwater percolation and infiltration ice formation associated with high surface melt rates modified the stratigraphy of firn in the ice cap's accumulation area very substantially. Growth of a 0.5-4.5 m thick ice layer that filled much of the pore volume of the upper part of the firn reduced vertical percolation of meltwater into deeper parts of the firn. This progressively limited the water storage potential of the firn reservoir, and likely caused a significant increase in surface runoff. An evaluation of the snowpack model Crocus against ground observations for the period 2004-2012 showed that, although the model simulated observed density/depth profiles relatively well at all sites, its representation of

heterogeneous percolation as a homogeneous process created conditions that favoured excessive near-surface freezing. At the same time, Crocus's parameterization of the permeability of ice layers forced meltwater to percolate through them, preventing the buildup of thick impermeable ice layers. These results highlight the importance of treating meltwater percolation in firn as a heterogeneous process, and of accurately representing the impermeability of ice layers to meltwater flow, if the model is to accurately reproduce firn density profile evolution and surface runoff during periods of climate warming.

Acknowledgments

First and foremost, I would like to thank my advisors, Dr. Martin Sharp and Dr. Andy Bush. Thank you for having given me the freedom to design a project I liked. Thank you, Martin, for your constant help and guidance, and your attention to detail; thank you for having been so generous of your time. I appreciated being challenged and stimulated by our discussions. I am also grateful for the numerous opportunities you have given me during my PhD. Thank you, Andy, for your guidance and help, especially while teaching the Atmospheric Modelling course for the first time.

I also thank Dr. Jeff Kavanaugh for his guidance and advice while at the University of Alberta, and for the amazing opportunity to lecture on the Juneau Icefield Research Project. It was definitely a breathtaking and stimulating experience.

Fieldwork on the Devon Ice Cap was a big component of my thesis. As such, I would like to thank many people, organizations, and funding agencies that participated, supported, and funded the program.

I had the opportunity to work with amazing people over the course of the four field seasons I was involved with. Many thanks to Angus Duncan, Brad Danielson, Colleen Mortimer, Dave Burgess, Hannah Milne, Ian Scriver, Martin Sharp, Peter Bezeau, Tyler de Jong, and Wesley Van Wychen, for having shared many adventures on the Devon Ice Cap with me. Having the opportunity to work with such an exceptional group people made my experience on the Devon Ice Cap stimulating, positive, and memorable. Many thanks to the past member of the Devon field team for having maintained and collected valuable data.

Permission to conduct research on the Devon Ice Cap was kindly granted by the Nunavut Research Institute and the communities of Grise Fjord and Resolute Bay. Fieldwork was funded by a NSERC Discovery Grant and Northern Research Supplement to M. Sharp, and by Canadian Circumpolar Institute and Northern Scientific Training Program grants.

The numerical modelling aspect of my studies would not have been possible without the guidance of Samuel Morin and Mathieu Lafaysse from Météo-France, Grenoble, as well as the formidable work from the WestGrid support team.

Many friends in Edmonton have helped and supported me during my studies. Alex Gardner, Ben Gready, and Angus Duncan were cheerful and dynamical officemates during the first part of my PhD. I appreciated the friendship of Hannah Milne, Brad Danielson, Colleen Mortimer, Fay Wyatt, Ian Scriver and

Peter Bezeau. A special thanks to my friends Louise, Alexandra, Magali, and Katarina, especially for French TV night and fun Zumba times.

Many, many, many thanks to my family, Papa and Sylvie, Maman and Maurice, Camille, and Èlise, who encouraged and supported me throughout my studies. Thank you for believing I could do it. I also thank Peter for brainstorming ideas, and for your love and support. I am grateful to have met you.

Finally, I would like to thank NSERC Canada, the Alberta Ingenuity Fund, the Fonds de Recherche du Quebec – Nature et Technologies (FQRNT), the Canadian Circumpolar Institute, the Institute of Geophysical Research of the University of Alberta, the University of Alberta, and the Canadian Meteorological and Oceanic Society (CMOS) for scholarships and grants throughout my degree.

Table of Contents

List of Tables

List of Figures

Chapter 1
Introduction

1.1 Background

Since the beginning of the 21st century, glaciers, ice caps, and ice sheets around the world have been losing mass at an increasingly rapid rate [e.g.: *Hanna et al.*, 2008; *Rignot et al.*, 2011; *Sharp et al.*, 2011; *Gardner et al.*, 2011, 2013]. Cumulative precipitation is the main influence on snow accumulation (mass gain), whereas sublimation, surface runoff, iceberg calving, and undermelt of floating ice shelves and tidewater glacier termini contribute to snow/ice ablation (mass loss) [e.g. *Cuffey and Paterson*, 2010; *Cogley et al.*, 2011]. Glaciers gain mass when their mass balance is positive, and lose mass when it is negative [*Cogley et al.*, 2011]. Glacier mass balance is controlled by environmental conditions, and the retreat-advance cycles of glaciers are, with the exception of surges, usually an effective indicator of changing climate.

In the Canadian Arctic Archipelago (CAA), inter-annual variability in the net surface mass balance of glaciers and ice caps is largely due to variability in the summer surface mass balance [*Koerner*, 2005]. The summer surface mass balance is directly correlated with summer surface air temperatures, and is influenced by the components of the surface energy balance, in particular the shortwave and longwave radiation budgets, and the latent and sensible heat fluxes. These energy balance terms are influenced by the environmental conditions in a glaciated area (air temperature, cloudiness, surface albedo, wind, humidity, etc.), which can, in turn, vary as a result of surface melting. Atmospheric circulation variability influences regional summer mean air temperatures in the Arctic [*Graversen et al.*, 2008], which in turn influence the surface mass and energy balances of glaciated regions [*Braun et al.*, 2001]. In the CAA, anticyclonic conditions in summer tend to be associated with high rates of melt, while cyclonic systems can be associated with either low or high melt rates [*Alt*, 1978; 1987]. *Wang et al.* [2005] demonstrated that, between 2000 and 2004, longer melt seasons tended to occur on glaciers and ice caps in the Canadian Arctic in years with above average July 500 hPa geopotential height, which implies strong anticyclonic conditions. More recently, the occurence of persistent anticyclonic conditions over the Greenland Ice Sheet and the eastern Canadian Arctic has been suggested to be a driving mechanism for more intense melt seasons [e.g.: *Sharp et al.*, 2011*; Fettweis et al.*, 2013; *Tedesco et al.*, 2013].

One corollary of the increased mass loss from glaciers, ice caps, and ice sheets since the beginning of the 21st century is an increase in the amount of surface melt in the accumulation areas of these ice masses [*Mote*, 2007; *Fettweis et al.*, 2011]. Unlike in the ablation area where surface meltwater is removed from the glacier by surface runoff, and/or drainage through englacial and subglacial channels, meltwater may percolate into firn in the accumulation area and refreeze. Heterogeneous percolation and refreezing of meltwater have been observed to depths of at least 10 m below the ice sheet surface in Greenland [*Humphrey et al.*, 2012], and it has been suggested that these processes may buffer the Greenland Ice Sheet's contribution to sea-level rise [*Harper et al.*, 2012]. An increase in surface melt in the accumulation area of glaciers will initially increase the amount of percolating meltwater that refreezes in the shallow subsurface layer of firn. This process may account for recent observations in the accumulation area of the Devon Ice Cap, Nunavut, Canada, where comparisons of density profiles in firn cores drilled in 2004 and 2012 showed increases of 13-80% in the densification rate of the top 2.5 m of the firn column over the intervening time interval [*Bezeau et al.*, 2013]. With time, however, refreezing of meltwater in firn will increase the number and thickness of ice layers in the firn, and may force the migration of the boundaries of the superimposed ice zone to higher elevations [*Bezeau et al.*, 2013]. It will also progressively reduce the water storage potential and refreezing capacity of the firn layer of the ice cap. The associated loss of firn pore volume has the potential to cause an acceleration of mass loss in the 21st century, even under constant climate conditions [*van Angelen et al.*, 2013].

1.2 Motivation

The CAA contains one-third of the global volume of land ice outside Greenland and Antarctica [*Radić and Hock*, 2011]. From 1963 to the end of the 20th century, surface temperatures and the mass balance of glaciers and ice caps in the Canadian Arctic showed little variability, with only a weak trend to summer warming and increasingly negative climatic mass balances that started around 1987 and accelerated after 1998 [*Braithwaite, 2005*; *Koerner, 2005*]. Since 2005, rapid increases in summer air temperature have been accompanied by higher rates of summer melt and increasingly negative climatic mass balances on the region's glaciers and ice caps [*Sharp et al*., 2011]. Strong summer warming since 2005 has increased the 2005-2009 summer mean air temperature over Canada's Arctic glaciers and ice caps by 0.8-2.2°C relative to 2000-2004 [*Sharp et al.*, 2011], and the rate of mass loss from this ice cover increased sharply from 31 Gt yr^{-1} for the 2004-2006 period, to 92 Gt yr^{-1} for the 2007-2009 period [*Gardner et al.*, 2011]. Outside Greenland and Antarctica, glaciers and ice caps in the CAA are currently the greatest regional contributor to eustatic sea-level rise [*Gardner et al*., 2011; 2013]

With summer Arctic surface temperatures expected to increase by at least 5°C over the next century [*Meehl et al.*, 2012], surface melt on glaciers and ice caps in the CAA will most likely increase, and may become irreversible by the end of the 21st century [*Lenaerts et al.*, 2013]. In order to better constrain the magnitude of projected sea-level rise from the CAA, it is critical to understand the environmental mechanisms that enhance surface warming and melt, and how the projected increase in surface melt will change the capacity of firn to retain meltwater. One important aspect of this is to determine how changes in the relative frequency of different synoptic weather types contribute to the recent trends in summer mean air temperature and the climatic mass balance of Arctic glaciers, ice caps, and ice sheets. Another is to determine exactly how, and how rapidly, percolation and refreezing of surface meltwater in firn will fill available pore volume, reducing the capacity of firn to buffer the region's contribution to sea-level rise, and increasing the fraction of surface melt that runs off from the accumulation areas of glaciers and ice caps in the year in which it is produced.

1.3 Project and Objectives

The observed changes in environmental conditions in the CAA raise the following questions (amongst others):

1) How are changes in melt season characteristics related to changes in the Arctic atmospheric circulation?
2) How do climate-driven changes in surface melt influence the stratigraphy and hydrology of the firn layer?
3) If significant changes in firn stratigraphy are observed, are they accurately simulated by current snowpack models?

In an effort to answer these questions, data from an extensive field program established to monitor environmental conditions on the Devon Ice Cap, Nunavut, Canada were analyzed. With an area of ~14,000 km^2, the Devon Ice Cap is the third largest and most southerly ice cap in the Queen Elisabeth Islands (QEI) [*Dowdeswell and others*, 2004]. Since 2004, multiple field campaigns have been conducted on the ice cap as part of efforts to calibrate and validate the radar altimeter on board the European Space Agency's CryoSat-2 satellite [*Burgess and Sharp*, 2008*; Colgan et al.*, 2008]. Surface air temperature, wind speed and direction, and relative humidity have been monitored since 2004, and surface radiation and albedo since 2007 at sites spanning a 1300 m elevation range along a 48 km transect that passes through all major facies zones in the accumulation area (the percolation, wet snow, and superimposed ice zones), and glacier ice in the ablation area on the south side of the ice cap. A total of 36 firn cores have been drilled since 2004, and repeated ground-penetrating radar (GPR) surveys have been conducted along the transect since 2007.

Although specific types of atmospheric circulation patterns are known to promote surface melt in the CAA [*Alt*, 1978, 1987; *Wang et al.*, 2005; *Sharp et al.*, 2011], the role of changes in the relative frequency of different synoptic weather types in the recent trends in summer mean air temperature and the surface mass balance of the region's glaciers has yet to be established. In order to do so, observations from three automatic weather and net radiometer stations were first analyzed to identify changes in melt season duration and surface energy balance on the Devon Ice Cap over the 2004-2010 period. Data from the North American Regional Reanalysis [*Mesinger et al.*, 2006] were then used to investigate possible shift in the dominant Arctic atmospheric circulation pattern over the intervening time interval. This work allows us to relate changes in surface melt characteristics with changes in the dominant synoptic weather patterns. Detailed descriptions of these results are presented in Chapter 2, which has been published in *Annals of Glaciology*. Although this article is co-authored, I performed all the analysis and wrote the entire manuscript; co-authors provided data used in the analysis that were collected prior to the beginning of my program.

Bezeau et al. [2013] documented changes in firn stratigraphy on the accumulation area of the Devon Ice cap using shallow ice cores drilled in two field seasons (2004 and 2012). Although their work documented rapid firn densification over that period, their study provided little insight into how the stratigraphy of the firn body as a whole developed over the intervening eight year period, or into how changes in firn stratigraphy were related to evolving patterns of water flow and storage within the firn layer. In order to address these issues, 500 MHz ground-penetrating radar (GPR) surveys conducted along a 40-km transect in each spring from 2007 to 2012 are analyzed. Four 190 m by 100 m GPR grid surveys performed in 2012, and 36 firn cores drilled between 2007 and 2012 supplement these linear GPR surveys and used to validate interpretations of along-transect changes in the radar stratigraphy. Our uniquely high-resolution dataset allows us to track the migration of the boundaries between the ice cap's major facies zones (superimposed ice, wet snow, and percolation zones) over time, describe the annual changes in firn stratigraphy associated with increased meltwater production, percolation, and refreezing since 2005, and explore the two-way interactions between changes in firn stratigraphy and meltwater storage and drainage patterns within the firn layer over time. Detailed description of these results is presented in Chapter 3, which has been published in *Journal of Geophysical Research (Earth Surface)*. Although this article is co-authored, I performed all the analysis and wrote the entire manuscript; co-authors provided data used in the analysis that were collected prior to the beginning of my program.

GPR surveys showed that changes in the firn stratigraphy of the Devon Ice Cap were rapid and widespread. Rapid densification and ice layer thickening appear to have progressively reduced the water storage potential of the firn layer, and may have led to an increase in the fraction of meltwater that runs off from the accumulation area of the ice cap, enhancing mass loss from the ice cap (see Chapter 3). Since refreezing parameterizations are included in models that are being used to predict future glacier mass balance and sea level change [e.g. *van Angelen et al.*, 2013], it is critical to determine whether they are capable of simulating changes in firn processes that are as large and rapid as those observed in the accumulation area of the Devon Ice Cap since 2005. In the absence of direct observations, refreezing parameterizations have been validated by comparing them against each other [*Reijmer et al.*, 2012]. Although that study showed that the six tested refreezing parameterizations agreed with each other, it is impossible to determine whether these parameterizations actually represent the magnitude and distribution of refreezing without evaluation against observations. Chapter 4 therefore presents results from an evaluation of the ability of the snowpack model Crocus [*Vionnet et al.*, 2012] to simulate the evolving firn stratigraphy recorded in 14 cores drilled at 4 elevations in the accumulation zone of the Devon Ice Cap between 2004 and 2012. This chapter has also been submitted to the *Journal of*

Glaciology. Although this article is co-authored, I performed all the analysis and wrote the entire manuscript; co-authors provided data used in the analysis that were collected prior to the beginning of my program, and access to Crocus' code.

Results from this thesis adds significantly to our knowledge of recent changes in melt conditions over glaciers and ice caps in the Canadian Arctic and their relationship to climate variability, and provides the first validation of the ability of firn densification models to capture these changes. Building on work by *Bezeau et al.* [2013], this project also documents climate-driven changes in firn stratigraphy and their implications to meltwater flow patterns within firn in the accumulation area of the Devon Ice Cap, Nunavut, during the 21st century summer warming. Chapter 5 summarizes the conclusion of the thesis, and discusses their implications for future work.

1.4 References

Alt, B.T. (1978), Synoptic Climate Controls of Mass-Balance Variations on Devon Island Ice Cap. *Arctic Alpine Res.*, 1, 61-80.

Alt, B.T. (1987), Developing synoptic analogues for extreme mass balance conditions on Queen Elizabeth Island ice caps, *J. Clim. Appl. Meteorol.*, 26, 1605– 1623.

Bezeau, P., M. Sharp, D. Burgess, and G. Gascon (2013), Firn profile changes in response to extreme 21st century melting at Devon Ice Cap, Nunavut, Canada, *J. Glaciol.*, 59(217), 981-991, doi:10.3189/2013JoG12J208.

Braithwaite, R.J. (2005), Mass balance characteristics of arctic glaciers, *Ann. Glaciol.*, 42, 225-229, doi:10.3189/172756405781812899.

Braun M, H. Saurer, S. Vogt, J.C. Simoes, and H. Gobman (2001), The influence of large-scale atmospheric circulation on the surface energy balance of the King George Island ice cap, *Int. J. Climatol.*, 21: 21–36.

Burgess, D.O. and M. Sharp (2008), Recent changes in thickness of the Devon Island ice cap, Canada, *J. Geophys. Res.*, 113, B07204, doi:10.1029/2007JB005238.

Colgan, W., J. Davis, and M. Sharp (2008), Is the high elevation region of the Devon Island ice cap thickening?, *J. Glaciol.*, 186, 428-436.

Cogley, J.G., R. Hock, L.A. Rasmussen, A.A. Arendt, A. Bauder, R.J. Braithwaite, P. Jansson, G. Kaser, M. Möller, L. Nicholson and M. Zemp (2011), Glossary of Glacier Mass Balance and Related Terms, IHP-VII Technical Documents in Hydrology No. 86, *IACS Contribution*, No. 2, UNESCO-IHP, Paris.

Cuffey, K.M., and W.S.B. Paterson (2010), The Physics of Glaciers, 4th edition. Academic Press, 704 pp.

Dowdeswell, J.A., T.J. Benham, M.R. Gorman, D. Burgess, and M.J. Sharp (2004), Form and flow of the Devon Island Ice Cap, Canadian Arctic, *J. Geophys. Res.*, 109, F02002, doi:10.1029/2003JF000095.

Fettweis, X., M. Tedesco, M. van den Broeke, and J. Ettema, (2011), Melting trends over the Greenland ice sheet (1958–2009) from spaceborne microwave data and regional climate models. C*ryosphere*, 5, 359–375.

Fettweis, X., E. Hanna, C. Lang, A. Belleflamme, M. Erpicum, and H. Gallée (2013), Brief communication "Important role of the mid-tropospheric atmospheric circulation in the recent surface melt increase over the Greenland ice sheet", *Cryosphere*, 7, 241-248, doi:10.5194/tc-7-241-2013.

Gardner, A.S., G. Moholdt, B. Wouters, G. J. Wolken, D. O. Burgess, M. Sharp, J. G. Cogley, C. Braun, and C. Labine. (2011), Sharply increased mass loss from glaciers and ice caps in the Canadian Arctic Archipelago, *Nature*, 473(7347), 357-360.

Gardner, A. S., G. Moholdt, J.G. Cogley, B. Wouters, A.A. Arendt, J. Wahr, E. Berthier, R. Hock, W.T. Pfeffer, G. Kaser, S.R.M. Ligtenberg, T. Bolch, M. J. Sharp, J.O. Hagen, M.R. van den Broeke and F. Paul (2013), A Reconciled Estimate of Glacier Contributions to Sea Level Rise: 2003 to 2009. *Science*, 340, 852-857.

Graversen, R. G., T. Mauritsen, M. Tjernstrom, E. Kallen, E., and G. Svensson (2008), Vertical structure of recent Arctic warming, *Nature*, 451, 7174, 53–56, doi:10.1038/nature06502.

Hanna, E., P. Huybrechts, and K. Steffen (2008), Increased runoff from melt from the Greenland ice sheet: A response to global warming, *J. Climate*, 21, 331–341, doi:10.1175/2007JCLI1964.1.

Harper, J., N. Humphrey, W. Pfeffer, J. Brown, and X. Fettweis (2012), Greenland contribution to sea level rise buffered by meltwater storage in firn, *Nature*, 491, 240-243.

Humphrey, N.F., J.T. Harper, and W.T. Pfeffer (2012), Thermal tracking of meltwater retention in Greenland's accumulation area, *J. Geophys. Res.*, 117, F01010, doi:10.1029/200JF002083.

Koerner, R. M. (2005), Mass balance of glaciers in the Queen Elizabeth Islands, Nunavut, Canada, *Ann. Glaciol.*, 42, 417–423, doi:10.3189/1727564057818 13122.

Lenaerts, J.T.M., J.H.V. Angelen, M.R.V. den Broeke, A.S. Gardner, B. Wouters, and E.V. Meijgaard (2013), Irreversible mass loss of Canadian Arctic archipelago glaciers, *Geophys. Res. Lett.*, 40, 1–5, doi:10.1002/ grl.50214.

Meehl, Gerald A., and Coauthors (2012), Climate System Response to External Forcings and Climate Change Projections in CCSM4. *J. Climate*, 25, 3661–3683. doi: http://dx.doi.org/10.1175/JCLI-D-11-00240.1

Mesinger, F., and Coauthors (2006), North American Regional Reanalysis, *Bull. Amer. Meteor. Soc.*, 87, 343–360. doi: http://dx.doi.org/10.1175/BAMS-87-3-343.

Mote, T. L. (2007), Greenland surfacemelt trends 1973–2007: evidence of a large increase in 2007, *Geophys. Res. Lett.*, 34, L22507.

Radić V. and R. Hock. 2010. Regional and global volumes of glaciers derived from statistical upscaling of glacier inventory data. *J. Geophys. Res*., 115, F01010, doi:10.1029/2009JF001373.

Reijmer C.H., M.R. Van den Broeke, X. Fettweis, J. Ettema, L.B.and Stap (2012), Refreezing on the Greenland ice sheet: a comparison of parameterizations. Cryosphere, 6(4), 743–762, doi: 10.5194/tc- 6-743-2012.

Rignot, E., I. Velicogna, M.R. van Den Broeke, A. Monaghan, and J.T.M. Lenaerts (2011), Acceleration of the contribution of the Greenland and Antarctic ice sheets to sea level rise, *Geophys. Res. Lett.*, 38, L05,503, doi:10.1029/2011GL046583.

Sharp, M., D.O. Burgess, J.G. Cogley, M. Ecclestone, C. Labine, and G.J. Wolken (2011), Extreme melt on Canada's Arctic ice caps in the 21st century, *Geophys. Res. Lett.*, 38, L11501, doi:10.1029/2011GL047381.

Tedesco, M., X. Fettweis, T. Mote, J. Wahr, P. Alexander, J.E. Box, and B. Wouters (2013), Evidence and analysis of 2012 Greenland records from spaceborne observations, a regional climate model and reanalysis data, *Cryosphere*, 7, 615-630, doi:10.5194/tc-7-615-2013.

van Angelen, J. H., J. T. M. Lenaerts, M. R. van den Broeke, X. Fettweis, and E. van Meijgaard (2013), Rapid loss of firn pore space accelerates 21st century Greenland mass loss, *Geophys. Res. Lett.*, 40, doi:10.1002/grl.50490.

Vionnet, V., E. Brun, S. Morin, A. Boone, S. Faroux, P. Le Moigne, E. Martin, and J.-M. Willemet (2012), The detailed snowpack scheme Crocus and its implementation in SURFEX v7.2, *Geosci. Model Dev.*, 5, 773-791, doi :10.5194/gmd-5-773-2012.

Wang, L., M.J. Sharp, B. Rivard, S. Marshall, and D. Burgess. 2005. Melt season duration on Canadian Arctic ice caps, 2000–2004, *Geophys. Res. Lett.*, 32, L19502, doi:10.1029/2005GL023962.

Chapter 2

Changes in melt season characteristics on the Devon Ice Cap, Canada, and their association with the Arctic atmospheric circulation[1]

2.1 Introduction

Inter-annual variability in the net surface mass balance of glaciers in Canada's Queen Elizabeth Islands (QEI) is due largely to variability in the summer surface mass balance [*Koerner*, 2005], which is directly correlated with variability in summer surface air temperatures. From 1963 until the end of the 20th century, there was little variability in either the summer mean surface air temperature or the mass balance of glaciers and ice caps in the QEI, and only a weak trend towards warmer summers and increasingly negative mass balances that started around 1987 and accelerated after 1998 [*Braithwaite*, 2005; *Koerner*, 2005; *Gardner and Sharp*, 2007]. Between 2005 and 2009, however, the summer mean surface air temperature over glaciers and ice caps in the QEI was 0.8-2.2 °C higher than the 2000-2004 average, and 30-48% of the total mass loss from 4 monitored glaciers since 1963 occurred in this period [*Sharp et al.*, 2011]. The annual rate of mass loss from all glaciers in the region increased sharply from ~31 Gt yr^{-1} in the period 2004-2006, to ~92 Gt yr^{-1} from 2007-2009 [*Gardner et al.*, 2011].

Atmospheric circulation variability influences both regional summer mean air temperatures and surface mass balance in the QEI. Anticyclonic conditions over the region in summer tend to be associated with high rates of melt, while cyclonic

[1] A version of this chapter has been published as Gascon, G., M. Sharp, A. Bush (2013), Changes in the melt season characteristics on Devon Ice Cap, Canada, in the 21st century, and their association with the Arctic atmospheric circulation, *Annals of Glaciology*, 54(63):101-110, doi: 10.3189/2013AoG63A601.

systems can be associated with either low or high melt rates [*Alt*, 1978]. High melt years tend to occur when a ridge intrudes from the south into the QEI, while low melt years are associated with a stationary deep cold trough that extends across the QEI and into Baffin Bay [*Alt*, 1987]. Negative mass balance anomalies prevail in years when the July Circumpolar Vortex is centered in the eastern Hemisphere, while positive anomalies occur in years when the vortex is strong and located in the western hemisphere [*Gardner and Sharp*, 2007]. *Wang et al.* [2005] suggested that inter-annual variations in summer melt duration in the period 2000-2004 were closely related to variations in the July 500 hPa height over the QEI, with longer melt seasons occurring in years with above average geopotential height. The occurrence of low-pressure systems over the region can alter the surface energy balance of glaciers by changing the net longwave and/or net shortwave radiation at the surface relative to what is observed under anticyclonic conditions. Cloudy conditions reduce the incoming shortwave radiation, but increase the incoming longwave radiation because a larger fraction of the outgoing longwave radiation is absorbed by the clouds and re-radiated back to the ground. However, the role of changes in the relative frequency of different synoptic weather types in the recent trends in summer mean air temperature and the surface mass balance of the region's glaciers has yet to be established and is the focus of this paper.

The ~14,000 km^2 Devon Ice Cap is the third largest and most southerly ice cap in the QEI [*Dowdeswell et al.*, 2004]. Between 2004 and 2010, ground-based measurements of meteorological conditions have been made at multiple locations spanning a 1300 m elevation range along a 47 km long transect that passes through all major snow facies zones on the south side of the ice cap (Figure 2-1). Here, these measurements are analyzed to determine trends in the surface air temperature and in the timing and length of the summer melt season, and to investigate the changes in glacier surface mass and energy balances. These are then related to changes in the Arctic atmospheric circulation

2.2 Methods

2.2.1 Field data collection

Devon Ice Cap is located on Devon Island, Nunavut, Canada. Between 2004 and 2010, measurements have been made by three Campbell Scientific automatic weather stations (AWS) located at elevations of 1800 m a.s.l. (Site 1; ice cap summit), 1400 m a.s.l. (Site 2) and 1000 m a.s.l. (Site 3). Surface air temperature was measured with 107B temperature probes mounted in 41303-5A radiation shields. The probes' sensors were Beta Therm 100K6A with a range of -50 °C to 50 °C and an accuracy ranging from ± 0.5 °C below -40 °C to ± 0.1 °C above 0 °C. Horizontal wind speed and direction were measured with R.M. Young 05103AP-10 Wind Monitor sensors with a range of 0 to 60 m s^{-1}. Accuracy is ± 0.3 m s^{-1} for the wind speed, and ± 3° for the direction. Relative humidity was measured using Vaisala HMP35CF relative humidity probes, that can operate in temperatures ranging from -20 °C to 60 °C and have an accuracy of ± 2 % (0-90% RH) to 3 % (90-100% RH). Surface elevation changes were measured by Campbell Scientific SR50 sonic rangers with measurement ranges of 0.5 to 10 m; accuracy is ± 0.01 m or 0.4%. All instruments were installed 1.5 to 2.0 m above the snow surface. Height of the sensor will be referred to as 2-m above the snow surface for all instruments since this is the average height of all sensors over the summer months. Measurements made every 2 seconds were averaged and stored every 2 hours for all instruments. Since the weather stations are serviced only once per year, typically between mid-April and the end of May, a sampling interval of 2 hours was chosen to allow the weather stations to remain operational all winter. In summer, the batteries were charged by a Campbell Scientific MSX20 solar panel providing 20 watts at peak output. Data were logged with Campbell Scientific CR10 or CR10x data loggers.

Surface air temperature was also measured using 4 Onset HOBO H8 Pro (H08-030-08) temperature sensors. Three of these were located at the AWS sites, and one was located at the ice cap margin at an elevation of 475 m (HB 47-4). The accuracy of these sensors is ± 0.25 °C. The sensors were installed in M-RSA

Onset radiation shields and recorded near surface (~ 1-2 m) air temperature at 10- (2004), 15- (2005-2006) and 30-minute intervals (2007-2010). The poles in the ablation area were expected to melt out so they were drilled deep into the ice. The HOBO sensors were thus initially installed near the surface so they would move up towards 2-m above the snow surface over time as ablation took place; all HOBOs sensors were installed at the same height along the surveyed transect for consistency. The Devon Ice Cap field site was visited twice per year (in the spring and fall) until 2007, allowing the opportunity to record data more frequently in summer and to change the AWS and sensor batteries in the fall. In 2007, it was decided to decrease the rate of the recording time interval to ensure continuous data logging throughout the winter season.

Shortwave and longwave radiation budgets, and surface albedo, were measured with Kipp and Zonen CNR1 net radiometers at Sites 1, 2 and 3 from 2007 to 2010. Incoming and reflected solar radiation were measured by two CM3 pyranometers, and surface albedo was determined as the ratio of reflected to incoming solar radiation. Incoming and outgoing far infrared radiation were measured in a similar manner using two CG3 pyrgeometers. CM3 and CG3 sensor accuracy is ± 10%. The CM3 sensors measure radiation in the spectral range of 305-2800 nm, while the CG3 sensors measure radiation in the spectral range of 5-50 μm. The sensors were installed at a height of 1.5 to 2 m above the snow surface, with sensors of each type oriented towards both the sky and the ground. Radiation and albedo measurements were made every 2 seconds, and averages were stored every 2 hours on CR10x data loggers. For summer 2009, only air temperature at Site 2 is available due to AWS, net radiometer and HOBO malfunction at Sites 1 and 3, and net radiometer failure at Site 2.

2.2.2 Two-meter air temperature processing

Two-meter air temperatures measured at Sites 1, 2 and 3 were averaged to daily and monthly values. Daily averages were computed by averaging measured 2-hourly air temperature over 24-hour periods (local time). Monthly average values are the averages of those daily averages over June, July and August. HOBO air temperature data were used when complete AWS records were not available (for all sites in 2004 and 2006, Site 2 in 2005, and Site 1 in 2007 and 2008). Air temperatures measured by the HOBO sensors were corrected to account for the instrument height differences compared to the height of the AWS temperature sensors. The linear regression relationship between air temperatures measured by the HOBO sensors and AWS temperature sensors was computed at each site for years when both datasets were available, and used to correct the air temperature at the sites for variations in instrument height. At Sites 1, 2 and 3, HOBO air temperatures were multiplied by 0.77, 0.97 and 0.91 (all $p<0.05$), respectively, and constants of 0.48, 0.34 and 0.60 °C, respectively, were added to the air temperature to ensure consistency with the AWS measured temperatures.

2.2.3 Energy balance modelling

The June-July-August (JJA) SEB was calculated as the sum of the net radiative (SW and LW) and turbulent (sensible and latent heat) fluxes. Both the subsurface heat flux and the sensible heat flux supplied by rain were neglected in this analysis. Fluxes were considered positive when directed towards the surface. Ice melt rates (cm w.e. d^{-1}/ yr^{-1}) were derived by dividing the melt energy by the latent heat of fusion of water and the density of liquid water [*Hock*, 2005].

The daily net radiation was computed by summing the measured 2-hourly recorded net longwave (incoming minus outgoing) and shortwave (incoming minus reflected) radiation fluxes. Penetration of shortwave radiation below the surface was ignored. The sensible and latent heat fluxes were calculated from AWS measurements of surface air temperature, relative humidity and wind speed at a single height using the bulk method [*Munro*, 1989; *Hock*, 2005]. Instrument height above the surface was determined using the SR50-measured height above the surface as all instruments on the weather station were installed at the same height. The surface roughness length was taken to be 0.0001 m for snow and 0.001 m for ice [*Alt*, 1975]. The surface was taken to be ice when the SR50 recorded a height above the surface greater than the winter snow accumulation measured at the end of May, after servicing the AWS and re-setting instrument heights. An empirical stability correction factor of 5, appropriate for stable conditions prevailing over glaciers and ice caps, was used in the calculation of the sensible and latent heat fluxes [e.g. *Holtslag and de Bruin*, 1988; *Klok et al.*, 2005]. Glacier surface temperature was calculated from the measured outgoing longwave radiation using the Stefan-Boltzman law on the assumption that snow and ice surfaces are black bodies with longwave emissivity of 1. The surface vapour pressure was set to the saturation vapour pressure at the calculated surface temperature if the surface temperature was below 0°C. When the surface temperature exceeded 0 °C, a saturation vapour pressure of 611 Pa was used as per the definition for surface conditions of a melting surface. Calculation of sensible and latent heat fluxes with the bulk method requires use of the Monin-Obukhov length scale *L* which requires prior knowledge of the sensible heat flux and the friction velocity. *L* was thus determined iteratively. For the first iteration, the sensible heat flux and friction velocity were calculated from measured data and derived for the location of the weather station using the neutral case. Calculated values of *L* were used in subsequent iterations. No significant changes in *L* occurred beyond 20 iterations.

2.2.4 Evaluation of atmospheric conditions

Data from the North American Regional Reanalysis (NARR) were used to characterize surface and upper-level pressure and geopotential height variability over the Canadian Arctic. NARR data are available for 29 distinct layers from 1979, and have high spatial (32 km) and temporal (three-hourly) resolution [*Mesinger et al.*, 2006].

Comparisons between the June, July and August mean upper-level (500 hPa) geopotential heights from NARR for the periods 2005-2010 period (strong warming) and 2000-2004 (more moderate warming) were used to illustrate changes in the atmospheric conditions over the QEI during the 21st century. In addition, the daily NARR surface (1000 hPa), near-surface (850 hPa) and upper-level (500 hPa) geopotential heights for June, July and August 2007, 2008 and 2010 were analyzed to identify and track specific weather patterns (cyclonic-anticyclonic systems) associated with periods of high melt energy at Site 2. The analysis of these weather patterns was then extended to the 2000-2010 period to investigate changes in their frequency since the beginning of the 21st century and their relationship to changes in mean monthly upper-level atmospheric conditions.

2.3 Results and discussion

2.3.1 Two-meter air temperature

Annual values of the summer mean 2-m air temperature (June-August average) and the monthly means for June, July and August are shown in Figure 2-2. At all sites, and for each month, 2-m air temperature increased from 2004 to 2010; trends are all significant ($p < 0.05$) except for JJA at Site 1, and August at Site 3. July had the warmest surface air temperatures in each year, and mean temperatures at Site 3 were above the melting point (0 °C) in that month in every year except 2004. August was usually warmer than June. The difference in monthly mean 2-m air temperature between the highest (Site 1) and lowest (Site 3) elevation stations ranged from 1°C in July 2006 and 2008, to 7°C in June 2007 and 2010. The smallest differences occurred in June-July 2006 (1°C) and July 2008 (1.4 °C). 2006 was a relatively cold summer in the Canadian Arctic, with the exception of August, which was warmer than the 2004-2010 average, with a mean 2-m air temperature similar to that recorded in 2010, the warmest year in the seven year record (Figure 2-2).

The summer daily mean 2-m air temperature increased from 2004 to 2010 (Figure 2-3). Surface air temperatures were continuously below the seven year average at all sites in 2004, while 2010 was the warmest of the seven years. Daily mean 2-m air temperatures were near the 2004-2010 average in 2005 and 2006, but above average in 2007 and 2008. This warming trend was previously reported by *Sharp et al.* [2011], and has been simulated with the Regional Climate Model Polar-WRF [*Gready*, 2012].

2.3.2 Melt season duration

The length of the melt season, melt onset and freeze-up dates, and the positive degree day (PDD) total were calculated for each site and year. The melt onset and freeze-up dates are defined by the first and last day with mean 2-m air temperature above 0 °C. A 5-day running mean of the mean 2-m air temperature was used to filter out single-day extremes. The melt season length is defined as the number of days between these two dates for each year and site. The melt duration, or number of melt days, was calculated by counting the number of days within each melt season with a mean 2-m air temperature above 0°C. Although a daily maximum 2-m air temperature above 0°C can occur on days with a mean 2-m air temperature below 0°C, we assume that melt water produced on such days will refreeze or percolate, leading to negligible daily net melt and mass loss. This approach may neglect surface runoff of meltwater, especially at Site 3 where winter accumulation is thinner and glacier ice is exposed faster. The PDD total was calculated by summing the daily mean 2-m air temperature for all days in a season when the average air temperature was positive. These values for the 3 sites are presented in Table 1 for each year from 2004 to 2010; period means and the annual rate of change of each parameter are also presented.

Melt duration ranged from 1 day or less at Sites 1 and 2 (2004-2005) to 76 days at Site 3 (2010). No day with a mean surface air temperature above 0 °C was recorded at Site 1 in 2004. Positive mean daily 2-m air temperatures were recorded in each melt season after 2005 at Site 2, and in each season after 2006 at Site 1. The single days with a temperature above 0 °C at Site 1 (0.1 °C) in 2005 and Site 2 (0.6 °C) in 2004 were assumed not to have produced significant net melt. Between 2004 and 2010, the timing of melt onset advanced by 0.3, 4.4 ($p<0.01$) and 4.5 days yr^{-1} at Sites 1, 2, and 3, respectively, for an average of 3 days yr^{-1} (non-significant). Similarly, the timing of freeze-up was delayed by 6.7, 5.4 ($p<0.05$) and 4.5 ($p<0.05$) days yr^{-1} at Sites 1, 2, and 3, respectively for a three-site average of 5.5 days yr^{-1}($p<0.05$). The 2010 melt duration at Site 1 was longer than the 2004 melt duration at Site 3. After 6 years of warming, 2-m air temperatures initially observed only at 1000 m a.s.l were being observed at 1800 m a.s.l., where there was no surface melt at the start of the period. The annual PDD total also increased significantly ($p<0.05$) over time at all sites, and increased with increasing melt season duration.

Between 2004 and 2010, an increase in melt duration has been observed at Sites 1-3 (Figure 2-4). Melt durations at Sites 2 and 3 after 2005-2006 are comparable to that at HB 47-7 in 2004. Site 1, located close to the Ice Cap summit, experienced the smallest increase in melt duration, suggesting that the warming has not yet raised mean daily air temperatures consistently above the melting point in summer at that location. The linear trends in melt duration from 2004 to 2010 were 3.4 ($p<0.1$; weak significance), 6.1 ($p<0.01$) and 8.8 ($p<0.05$) d a^{-1} at Sites 1, 2 and 3, respectively. In comparison, Sharp et al. (2011) reported that the QuikScat-derived mean annual melt duration over the entire Devon Ice Cap increased by an average of 4.7 days yr^{-1} between the periods 2000-2004 and 2005-2009.

2.3.3 Surface energy balance (SEB) analysis

Here, the SEB is calculated from the AWS and net radiometer data for Site 2 for 2007, 2008 and 2010. These are three of the four warmest years since 2004, both in the Canadian Arctic and on Devon Ice Cap (see Figure 2-3). Investigating the melt energy components during these years will allow us to identify specific SEB regimes associated with high melt years. SEB was calculated for Site 2 only since it is the sole site for which the net radiometer provided near-complete measurements.

Table 2 shows the June, July, August and JJA daily averaged values of net shortwave radiation, net longwave radiation, sensible and latent heat fluxes, daily averaged melt energy, and total monthly melt for the years 2007, 2008 and 2010 at Site 2. Figure 2-5 shows the daily net shortwave radiation, net longwave radiation, sensible and latent heat fluxes, and the daily averaged surface albedo at

Site 2 for the same years. The daily mean melt energy ranged from 23 to 58 W m^{-2}, representing a daily average melt rate of 0.6 - 1.5 cm w.e. d^{-1}. Net shortwave radiation was the main source of melt energy (50 to 102 W m^{-2} as a daily average), in agreement with previous studies in the high Arctic (e.g.: Braithwaite, 1981; Klok et al., 2005). The net longwave radiation was a sink of melt energy (-28 to -70 W m^{-2} as a daily average). The mean daily sensible heat flux, which ranged between 29 and 50 W m^{-2}, was the second largest source of melt energy. The large mean sensible heat flux is consistent with the large observed difference between the 2-m air temperature and the temperature of the air just above the surface, and the high summer mean daily surface wind speed (14 km hr^{-1}). The latent heat flux is an energy sink in the SEB, with an average daily value between -11 and -20 W m^{-2}. The Devon Ice Cap is a relatively dry environment, with a summer average relative humidity of 75%, which promotes evaporation and sublimation and reduces the contribution of the latent heat flux to surface melt. The average surface albedo decreases until around day of year 195 (mid-July) as the degree of metamorphism of surface snow increases and the underlying ice surface is eventually exposed. Thereafter, it exhibits oscillatory behavior, reflecting changes in surface condition between snow, bare ice, and ponded and refrozen meltwater.

The computed JJA melt at Site 2 increased progressively from 74, to 132, to 133 cm w.e. in 2007, 2008 and 2010 respectively. Changes in the net longwave, net shortwave and sensible heat flux components of the SEB are the main contributors to the observed increase in melt for each summer month (Table 2). The smallest variation in SEB occurred in June, where little variation in any of the components was observed. In July, an increase in net shortwave radiation from 86-85 W m^{-2} in 2007-2008 to 102 W m^{-2} in 2010, and a decrease in net longwave radiation in 2008 and 2010 (-46 and -49 W m^{-2}) compared to 2007 (-70 W m^{-2}) are responsible for the gradual increase in melt energy for that month. In August, the largest changes in SEB came from an increase in the net longwave radiation in 2008 and 2010 (-28 and -32 W m^{-2}) compared to 2007 (-54 W m^{-2}), and a 60%

increase in sensible heat flux in 2008 compared to 2007 and 2010. The latent heat flux contribution remained quasi-constant for each year and month.

The observed increase in melt energy from 2007 to 2010 is most marked in July and August, and is mainly due to an increase in net shortwave radiation (associated with lower surface albedo) in July, and an increase in net longwave radiation in August. As the net longwave radiation is a sink of energy for melt, its increase implies a reduced sink and an increase in the SEB. The increase in net longwave radiation is consistent with the observed increase in 2-m air temperature measured by the three weather stations on Devon Ice Cap, as a warmer atmosphere will increase the downwelling infrared radiation while the upwelling longwave flux is limited by the melting temperature of the snow/ice surface. In 2008, the high calculated melt energy was also due to a high value of the average sensible heat flux in August despite lower measured 2-m air temperature compared to 2007 and 2010. On Devon Ice Cap, the sensible heat flux is positively correlated with both the air temperature and the wind speed, and a higher daily averaged wind speed in August 2008 was responsible for the high calculated sensible heat flux (not shown).

Two different SEB regimes associated with high daily melt energy were identified and are observed in each year. The daily average values of each of the SEB components for all days in June, July and August 2007, 2008 and 2010 define the two high melt regimes (Figure 2-6). The first regime is characterized by consistently high net shortwave radiation (118 W m^{-2} average) and low net longwave radiation (-77 W m^{-2} average), with the high net shortwave radiation being the dominant component (Figure 2-6a); this leads to increased incoming energy. This regime is more common at the beginning of each melt season and is typical of the months of June and July (see Figure 2-5). The second regime is characterised by lower net shortwave radiation (average of 40 W m^{-2}) and higher net longwave radiation (average of -3.4 W m^{-2}) (Figure 2-6a). This regime is observed at the end of each melt season, typically following day of year 210 (July

29), and each individual period dominated by this regime lasted between 3 and 5 days. A third regime, associated with low melt energy, is characterized by lower values of all components of the SEB. In none of the three melt regimes do the turbulent fluxes have a dominant influence (Figure 2-6b-c). These fluxes also never account for more than 50% of the net daily melt energy in either June, July or August.

2.3.4 Accuracy and validation of SEB model

Each component of the calculated SEB is associated with measurement errors provided by the instrument manufacturers (see Field Site and Data section). The net radiometer instrument's accuracy of 10% led to a daily average error of ± 9 (range 1-17) W m^{-2} and ± 6 (range 2-10) W m^{-2} for the net shortwave and net longwave radiation, respectively. The calculations of the latent and sensible heat fluxes imply that there is a systematic error related to the input of each of the measured environmental variables (wind, 2-m air temperature, relative humidity). Using the propagation of error approach and the accuracy of each of the AWS instruments, we found that the daily average error associated with the calculation of the sensible heat flux was of ± 8 (range ± 1-24) W m^{-2}, and the daily average error associated with the calculation of the latent heat flux was of ± 5 (range ± 1-21) W m^{-2}; the daily average error associated with the calculation of the melt energy was ± 13 (range ± 2-35) W m^{-2}. The mean error associated with the calculation of the daily melt rate was then ± 0.003 cm w.e. (range ± 0.0004-0.009 cm w.e.). Cumulative JJA melt error was estimated to be ± 20, 17 and 26 cm w.e. for 2007, 2008 and 2010, respectively.

The calculated SEB melt is validated against melt measured directly by the SR50 instrument installed on the AWS at Site 2 (Figure 2-7). An average firn/ice density of 850 kg m^{-3} derived from shallow ice core measurements at Site 2 was used to convert the SR50 height measurements (in cm) into cm w.e. quantities. The SR50 measured a cumulative melt value of 75, 134 and 134 cm w.e., compared to 74, 132, and 133 cm w.e. for the calculated SEB melt in 2007, 2008 and 2010 respectively. For all three years, the cumulative melt derived from the SEB calculation is consistent with the value of the SR50 measured melt and its uncertainty. In 2007, both curves are consistent with each other, and the SEB model underestimates the cumulative melt at the end of the season by only ~ 1% compared to the SR50 value. The main difference between the two curves is the inability of the SEB model to capture the sharp melt event around day-of-year 190 (July 9) in 2007. In 2008, the two curves are very similar and overlie each other, with the SEB calculations consistently underestimating the SR50 measured melt by 1-2 %. We note that the SR50 failed temporarily between days of year 198 and 213 (July 16-August 1) without impairing the results. Although the cumulative melt derived from the SEB calculation is consistent with the SR50 measured melt at the end of the 2010 melt season, the two curves are not consistent with each other during one third of the melt season. By this time, the SR50 was then over 5 years old and, as shown by its multiple failures over the course of that melt season, its measurements may have been inaccurate.

2.3.5 Atmospheric conditions and their association with surface melt

Changes in the atmospheric circulation and short-term (2-5 days) weather patterns over the Canadian Arctic in June, July and August are clearly related to the observed increases in 2-m air temperature and melt season duration since 2004, and they are also a driving mechanism of the shifts in the nature of the SEB regime associated with periods of high melt.

Relative to 2000-2004, 2005-2010 was characterized by a positive 500 hPa geopotential height anomaly over the southern Canadian Arctic in June and July (Figure 2-8a). This anomaly defines a steeper and more persistent 500 hPa ridge associated with a strong anticyclonic circulation over the region. Based on the analysis of daily weather conditions, the occurrence of this upper level ridge in June and July was twice as high in 2005-2010 (average of 23 days yr^{-1}) as in 2000-2004 (average of 11 days yr^{-1}). In agreement with previous studies (Alt, 1987; Wang et al., 2005), these results suggest that the higher melt years observed in the period 2005-2010 are associated with a more persistent and steeper 500 hPa ridge than was present in the summers of 2000-2004. This anticyclonic circulation brings warm air into the Canadian Arctic from the south. The intensification of the ridge after 2004 signifies greater northward advection of warm air from the North American continent to the west of Hudson Bay, contributing to the observed increase in 2-m air temperature in June and July.

Anticyclonic circulations are also characterized by cloud-free conditions, and their intensification contributed to observed increase in SEB and melt energy. An increase in their intensity and persistence results in increased incoming shortwave radiation and progressively lower surface albedo (see Figure 2-5, day of year 170-190), primarily intensifying the SW component of the SEB and the overall melt energy (Figure 2-9a). This SEB regime is seen in June and July of 2007, 2008 and 2010. It is characteristic of the first high melt SEB regime identified in Figure 2-6, and is associated with the first periods of high melt in each year. It is responsible for a 4-24% increase in melt energy in June and July (Table 3) relative to June-July daily average.

A negative 500 hPa geopotential height anomaly was present over the QEI in the Augusts of 2005-2010 (Figure 2-8b). Such an anomaly implies an upper-level trough that is typically associated with surface low-pressure systems. When the upper-level trough extends to high enough latitudes, the associated surface systems travel north towards the QEI, and their advancing warm surface fronts advect warm and moist air into the Arctic from the south. Analysis of daily NARR 1000 hPa and 850 hPa geopotential height data shows that low-pressure systems arriving from the south-west and moving towards the north and north east reached the Canadian Arctic in every August of the 2005-2010 period (and once in late July in 2008). These systems had a lifetime of between 3 and 5 days. The Devon Ice Cap is located sufficiently far south to be influenced by this north-eastward transport of warm air. Only one or two such low-pressure systems were observed in each August of the 2000-2004 period, but they occurred more frequently (2-4 per year) and later in August between 2005 and 2010. The increase in occurrence of such systems contributed to the observed increase in 2-m air temperature, and their timing becoming progressively later in August can explain the end of the melt season becoming later by 4.5 to 6.7 days yr^{-1} during the period 2004 to 2010.

The SEB regime was also influenced by the occurrence of these south-westerly low-pressure systems. Indeed, a 12-38% increase in melt energy relative to the averaged August daily melt energy is associated with the occurence of such systems. This change in melt energy is mainly due to an increase in net longwave radiation and a decrease in net shortwave radiation lasting for the observed lifetime of the surface low-pressure systems (3 to 5 days) (Figure 2-9b, Table 2-3). Compared to the 2007-2010 August daily average, net longwave radiation increased by over 100% (and even became positive) during such low pressure conditions in 2008 and 2010. During the overcast conditions associated with low-pressure systems, clouds will absorb and re-emit longwave radiation, increasing the downwelling component of longwave radiation. At the same time, net shortwave radiation is reduced significantly relative to the 2007-2010 August daily average, due to blocking of incoming shortwave radiation by clouds. Such conditions are characteristic of the second high melt SEB regime identified in Figure 2-6 and are characterized primarily by the reduction in longwave radiation losses from the surface. At the same time, significant increases in the latent heat flux and decreases in the sensible heat flux were observed during low-pressure systems. This is consistent with an increase in relative humidity promoting condensation during precipitation events, and a surface temperature that is closer to the 2-m air temperature due to the mixing of the air column by strong winds during surface low-pressure systems.

2.4 Summary and conclusion

Changes in melt season characteristics at three elevations on the Devon Ice Cap were examined for the period 2004-2010. The SEB and melt rate were calculated for Site 2 for three years in the 2007-2010 period, and the observed changes in air temperature and SEB were linked with changes in the Arctic atmospheric circulation in the early 21st century.

A sharp increase in the summer mean surface air temperature occurred after 2004. Between 2004 and 2010, the timing of melt onset advanced by a three-site average of 3 days yr^{-1} (non-significant), and the timing of freeze-up was delayed by a three-site average of 5.5 days yr^{-1} ($p<0.05$). Over that same period, the melt season length increased by 3.4 ($p<0.1$; weak significance), 6.1 ($p<0.01$) and 8.8 ($p<0.05$) days yr^{-1} at 1800, 1400 and 1000 m a.s.l. respectively, and melt durations typical of ice marginal locations (475 m a.s.l; HB 47-7) in 2004 were observed at locations 900 m higher on the ice cap in 2010.

Associated with the observed increase in air temperature was an increase in calculated melt rates at Site 2 from 74 cm w.e. yr^{-1} in 2007, to 132 and 133 cm w.e. yr^{-1} in 2008 and 2010, consistent with direct measurements of melt at the same location. Although each component of the SEB contributed to the increased melt, two distinct SEB regimes associated with high melt rates were identified: one associated with high net shortwave radiation in June and July, and one with relatively high net longwave radiation and reduced net shortwave radiation in August. These were associated with distinctive features of the Arctic atmospheric circulation.

A steeper and more persistent 500 hPa ridge associated with a strong anticyclonic circulation over the region in June and July 2005-2010 accounted for the higher observed 2-m air temperature and calculated melt in June and July. This was was associated with greater net shortwave radiation, which promoted rapid metamorphism and eventual removal of the snow, decreased the mean surface albedo, and increased the melt energy available early in the season by 4-24% between 2007 and 2010.

In August, increased occurrence of south-westerly low-pressure systems in 2005-2010 compared to 2000-2004 delayed the end of the melt season over the Devon Ice Cap by an average of 5.5 days yr^{-1} ($p<0.05$) at the three sites. These weather patterns enhanced surface melt by advection of warm air into the Arctic (which increased the melt energy derived from the turbulent fluxes and accounted for the observed increase in 2-m air temperature) and by increasing the net longwave radiation by enhancing its downwelling component via greater emission from more extensive cloud cover (even though it also decreased the net shortwave radiation by blocking incoming shortwave radiation). Under these conditions, melt energy increased by 12-38% between 2007 and 2010 compared to the August daily average. The changes in the summer atmospheric circulation over the Canadian Arctic are implicated in the recent increase in summer mean air temperature and in the sharp increase in melt energy and melt on the ice cap in the 21st century.

Tables

Table 2-1: 2004-2010 melt onset and freeze-up day (in day of year), melt duration (in days) and PDD total (in °C-days) (a) Site 1, (b) Site 2, and (c) Site 3. The last column to the right represents the 2004-2010 annual rate. (*) denotes single days with a temperature above 0 °C. For the melt onset and freeze-up rate, negative values represent an advance, and positive values, a delay. In the Rate (yr^{-1}) column, values underlined in bold are significant to $p<0.01$, values in bold are significant to $p<0.05$, and values in grey are significant to $p<0.1$.

AWS location	2004	2005	2006	2007	2008	2009	2010	Mean	Rate (yr^{-1})
Site 1									
Melt onset (day of year)	NA	190*	190	181	179	---	187	185	-0.3
Freeze-up (day of year)	NA	190*	228	200	225	---	238	216	6.7
Melt duration (days)	0	1	25	12	30	---	16	14	3.4
PDD total (°C-days)	0	0.1	38	11	69	---	20	23	**5.9**
Site 2									
Melt onset (day of year)	203*	189	191	178	175	192	165	184	**<u>-4.4</u>**
Freeze-up (day of year)	203*	210	230	223	223	224	237	221	**5.4**
Melt duration (days)	1	12	25	38	33	29	44	26	**<u>6.1</u>**
PDD total (°C-days)	0.6	8	34	51	52	51	68	38	**<u>10.9</u>**
Site 3									
Melt onset (day of year)	188	171	189	175	174	---	161	176	-4.5
Freeze-up (day of year)	205	223	231	228	224	---	241	225	**4.5**
Melt duration (days)	6	49	34	50	41	---	76	43	**8.8**
PDD total (°C-days)	4	50	61	146	114	---	235	102	**<u>36.4</u>**

Table 2-2: 2007, 2008 and 2010 monthly averages of daily averaged net shortwave radiation, net longwave radiation, sensible heat flux (SHF), latent heat flux (LHF), and daily averaged melt energy for June, July, August and June-July-August at Site 2. Melt (cm w.e.) is the total monthly and JJA values for the years 2007, 2008 and 2010. Value in brackets is the averaged calculated uncertainty. (*) Cumulative JJA melt uncertainty is ± 20, 17 and 26 cm w.e. for 2007, 2008 and 2010, respectively.

SEB components	June			July			August			JJA		
	2007	2008	2010	2007	2008	2010	2007	2008	2010	2007	2008	2010
SW_{net} (±9 W m^{-2})	65	66	71	86	85	102	62	50	60	71	67	77
LW_{net} (±6 W m^{-2})	-55	-49	-50	-70	-46	-49	-54	-28	-32	-60	-41	-44
SHF (±8 W m^{-2})	43	45	40	37	33	40	29	50	29	36	43	35
LHF (±5 W m^{-2})	-16	-15	-16	-20	-15	-17	-14	-14	-11	-17	-15	-15
Melt energy (±13 W m^{-2})	37	47	45	33	57	76	23	58	46	31	54	53
Melt (cm w.e.)*	30	38	35	26	48	61	18	46	37	74	132	133

Table 2-3: Relative changes (in %) of the daily net shortwave radiation, net longwave radiation, sensible heat flux (SHF), latent heat flux (LHF), and daily averaged melt energy and melt rate in for 2007, 2008 and 2010 between: (i) June-July averaged conditions and days associated with strong 500 hPa ridges (in June-July), characterizing SEB regime 1, and (ii) August averaged conditions and days associated with the passage of south-westerly low-pressure systems (in August), characterizing SEB regime 2.

SEB components	June-July			August		
	2007	2008	2010	2007	2008	2010
SW_{net} (% W m^{-2})	33	55	38	-48	-22	-33
LW_{net} (% W m^{-2})	28	67	38	69	105	112
SHF (% W m^{-2})	10	-5	10	-23	-50	-4
LHF (% W m^{-2})	33	25	25	52	85	61
Melt energy (% W m^{-2})	19	4	24	17	12	38
Melt rate (% cm w.e.)	19	4	24	17	12	38

Figures

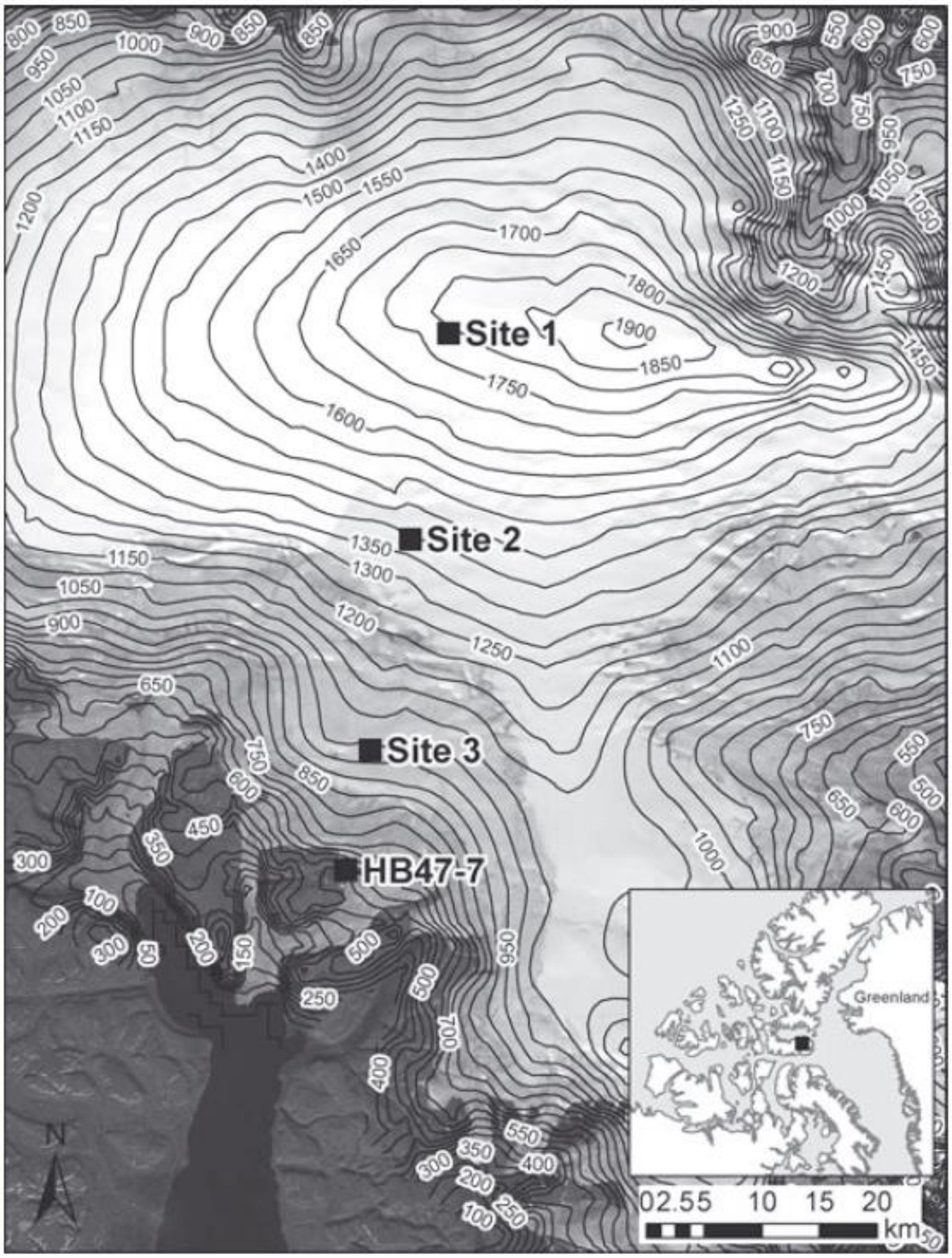

Figure 2-1: Weather stations, net radiometers and HOBO temperature sensor distribution on Devon Ice Cap. Weather stations, net radiometers and three of the HOBOs are located at Sites 1, 2 and 3. The southernmost HOBO sensor is designated by the letters HB followed by its distance (km) away from Site 1. Contour intervals are of 50 meters.

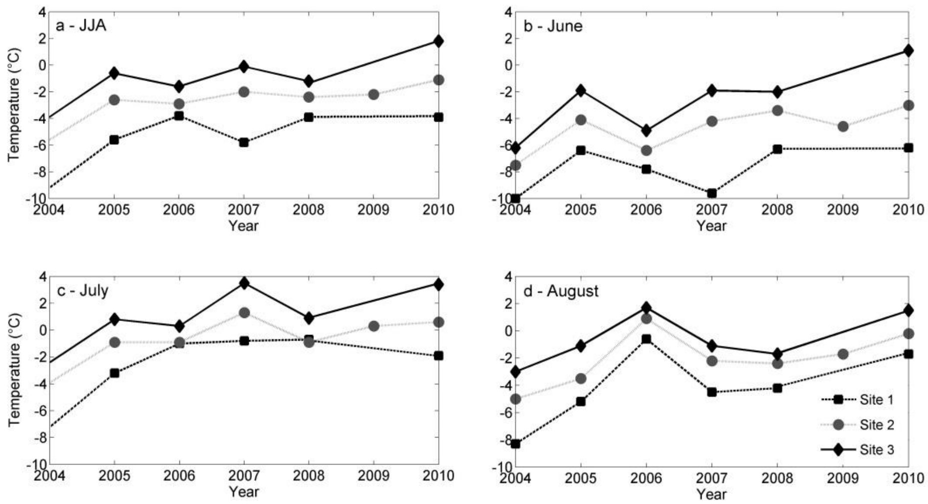

Figure 2-2: Average 2-m air temperature at Site 1 (square), Site 2 (circle), Site 3 (diamond) for (a) June-July-August, (b) June, (c) July and (d) August.

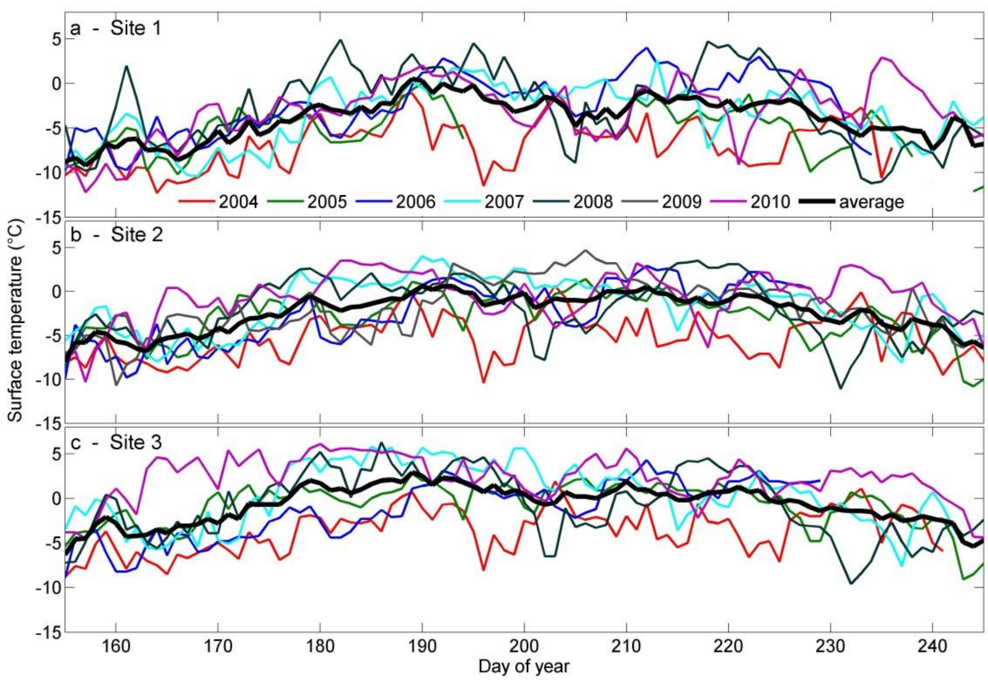

Figure 2-3: Time series of the daily average surface temperature at (a) Site 1, (b) Site 2, and (c) Site 3. The thick black line represents the 2004-2010 daily average.

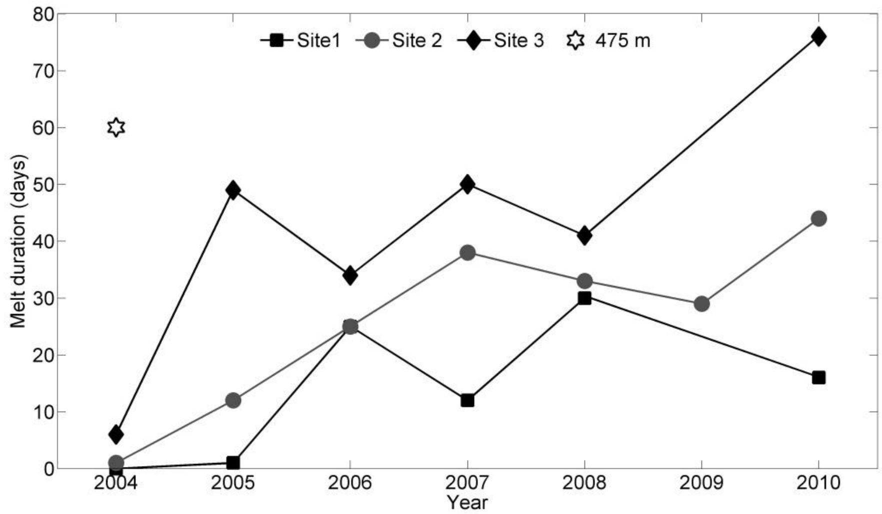

Figure 2-4: Melt duration (in days) between 2004 and 2010 for Site 1 (square), Site 2 (circle), and Site 3 (diamond). The 2004 HOBO-derived melt duration at site HB 47-7 at 475-m a.s.l. elevation (white star) is also shown.

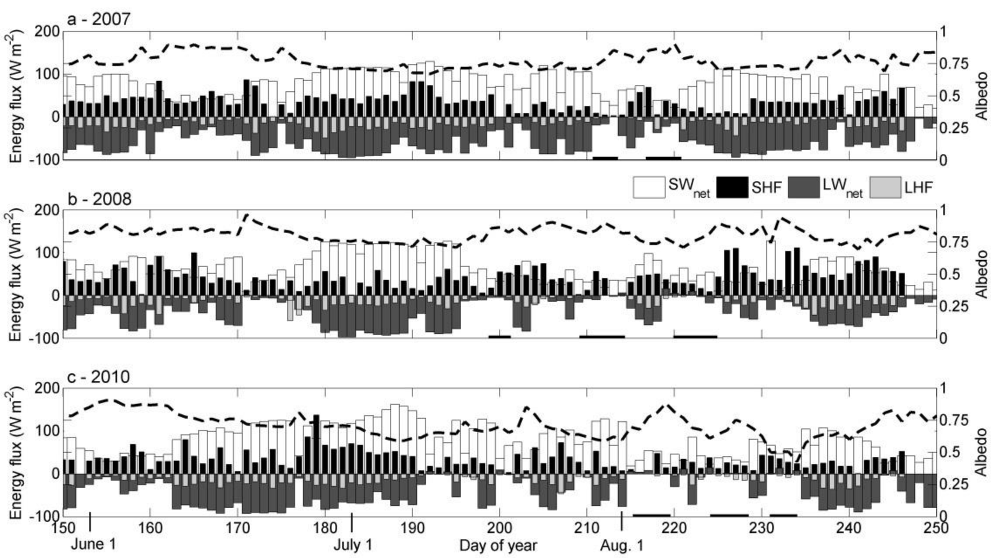

Figure 2-5: Daily averages of net surface short wave (*SW_{net}*), net surface longwave radiation (*LW_{net}*), sensible heat flux (*SHF*), and latent heat flux (*LHF*) at Site 2 in (a) 2007, (b) 2008, and (c) 2010. Daily average of surface albedo (black line) is also plotted. The period is for day of year 150 (May 30) to 250 (September 7). The black lines identify periods associated with the second high melt SEB regime.

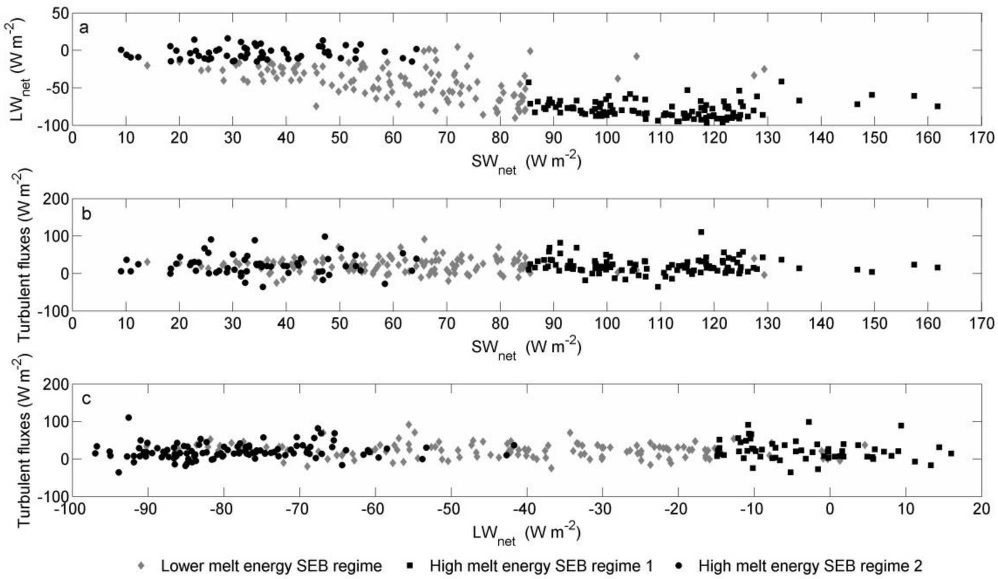

Figure 2-6: Daily average contribution of (a) net surface short wave (SWnet) against net surface longwave radiation (LWnet), (b) net surface short wave (SWnet) against turbulent fluxes, and (c) net longwave (LWnet) against turbulent fluxes in June, July and August 2007, 2008 and 2010. The black squares (on the right) and black circles (on the left) represent two different combinations of the SEB components associated with high melt energy. The black squares represent high SWnet and low LWnet, conditions associated with an anticyclonic circulation over the Canadian Arctic. The black circles are associated with high LWnet and low SWnet, and are typical of the occurrence of south-westerly low pressure systems. The grey diamonds represent the low melt regime, associated with lower values of each of the SEB components.

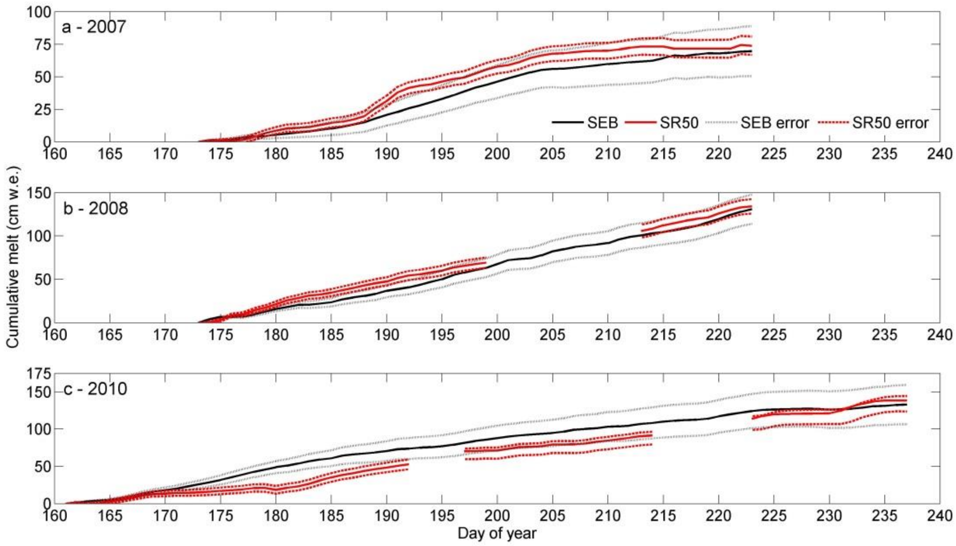

Figure 2-7: Cumulative melt calculated from the SEB (black) and derived from the SR50 instrument (red) at Site 2 for (a) 2007, (b) 2008, and (c) 2010. The black dotted line represents the cumulative error of the calculation of the SEB associated with measurement error. The red dashed line represents the cumulative measurement error of the SR50 instrument; cumulative error was ± 7 cm for 2007 and 2008, and ± 9 cm for 2010. Data gaps in 2008 and 2010 are due to brief malfunctions of the SR50.

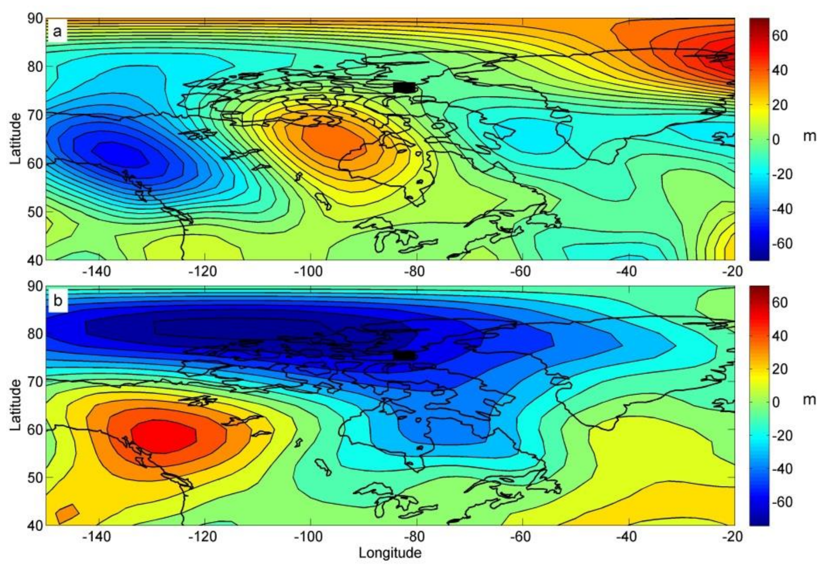

Figure 2-8: NARR 500 hPa geopotential height (m) difference between the 2005-2010 and the 2000-2004 period for (a) July, and (b) August. Devon Ice Cap is identified by the black rectangle. Contour intervals are every 5 m for (a), and every 10 m for (b).

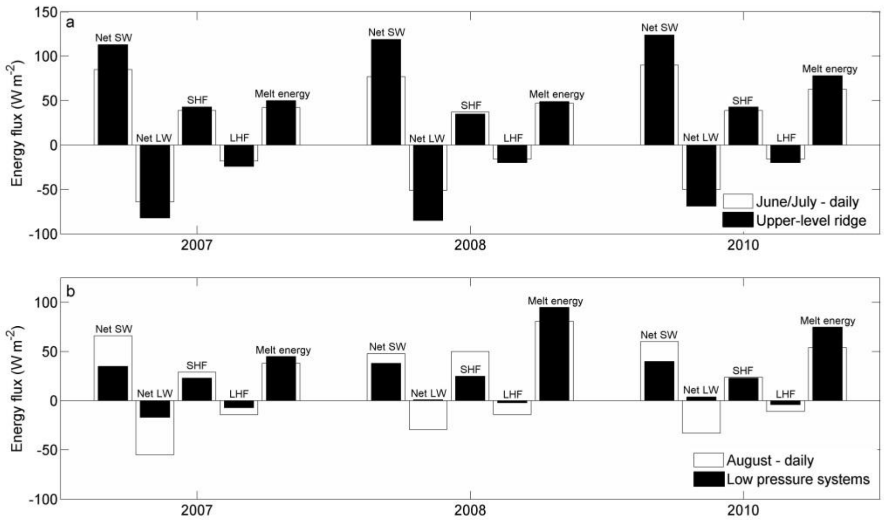

Figure 2-9: Daily averaged net surface short wave, net surface longwave radiation, SHF, LHF and melt energy in 2007, 2008, and 2010 for a) June-July daily averaged in white, and daily averages coinciding with the occurrence of a strong 500 hPa ridge in black, and b) August daily averages in white, and daily averages on days coinciding with the occurrence of low-pressure systems over the Canadian Arctic in black.

2.5 References

Alt, B.T. (1975), Energy balance climate of Meighen Ice Cap, N.W.T. *Polar Continental Shelf Project Monogr*. I, 64 pp., II, 101 pp.

Alt, B.T (1978), Synoptic Climate Controls of Mass-Balance Variations on Devon Island Ice Cap. *Arctic and Alpine Research*. 1, 61-80.

Alt, B.T. (1987), Developing synoptic analogues for extreme mass balance conditions on Queen Elizabeth Island ice caps. *J. Clim. Appl. Meteorol.*, 26, 1605– 1623.

Braithwaite, R.J. (1981), On glacier balance, ablation and air temperature. *J. Glaciol.*, 27, 381-391.

Braithwaite, R.J. (2005), Mass balance characteristics of arctic glaciers. *Ann. Glaciol.*, 42, 225-229, doi:10.3189/172756405781812899.

Dowdeswell, J.A., T.J. Benham, M.R. Gorman, D. Burgess, and M.J. Sharp (2004), Form and flow of the Devon Island Ice Cap, Canadian Arctic. *J. Geophys. Res.*, 109, F02002, doi:10.1029/2003JF000095.

Gardner, A.S., and M. Sharp (2007), Influence of the Arctic Circumpolar Vortex on the mass balance of Canadian High Arctic glaciers. *J. Clim.*, 20, 4586–4598.

Gardner, A.S., G. Moholdt, B. Wouters, G.J. Wolken, D.O. Burgess, M.J. Sharp, J.G. Cogley, C. Braun, and C. Labine (2011), Sharply increased mass loss from glaciers and ice caps in the Canadian Arctic Archipelago. *Nature*, 473(7347), 357-360.

Gready, B.P. (2012), Regional climate modeling over the Glaciers and Ice Caps of the Canadian Arctic and Greenland. PhD Thesis, University of Alberta.

Hock, R. (2005), Glacier melt: a review of processes and their modeling. *Progr. Phys. Geogr.*, 29(3), 362–291.

Holtslag, A.A.M. and H.A.R. de Bruin (1988), Applied modeling of the nighttime surface energy balance over land. *J. Appl. Meteorol.*, 27(6), 689–704.

Klok, E.J., M. Nolan, and M.R. van den Broeke (2006), Analysis of meteorological data and the surface energy balance of McCall Glacier, Alaska. *J. Glaciol,*. 51, 451–461.

Koerner, R.M. (2005), Mass balance of glaciers in the Queen Elizabeth Islands, Nunavut, Canada, *Ann. Glaciol*., 42, 417–423, doi:10.3189/172756405781813122.

Mesinger, F., et al. (2006), North American Regional Reanalysis. *Bull. Amer. Meteor. Soc.*, 87, 343–360. doi: http://dx.doi.org/10.1175/BAMS-87-3-343.

Munro, D.S. (1989), Surface roughness and bulk heat transfer on a glacier: comparison with eddy correlation. *J. Glaciol.*, 35(121), 343–348.

Sharp, M., D.O. Burgess, J.G. Cogley, M. Ecclestone, C. Labine, and G.J. Wolken (2011), Extreme melt on Canada's Arctic ice caps in the 21st century. *Geophys. Res. Lett.*, 38, L11501, doi:10.1029/2011GL047381.

Wang, L., M.J. Sharp, B. Rivard, S. Marshall, and D. Burgess (2005), Melt season duration on Canadian Arctic ice caps, 2000–2004. *Geophys. Res. Lett.*, 32, L19502, doi:10.1029/2005GL023962.

Chapter 3

Changes in the firn stratigraphy and meltwater flow pattern of the accumulation area of the Devon Ice Cap, Nunavut, Canada, during a period of climate warming[2]

3.1 Introduction

Canada's Queen Elizabeth Islands (QEI) contain one-third of the global volume of land ice outside Greenland and Antarctica [*Radić and Hock*, 2011], and glacier mass loss from this region is now a significant contributor to eustatic sea-level rise [*Gardner et al*., 2011, 2013]. A recent trend towards warmer summers and increasingly negative climatic mass balances of glaciers and ice caps in the QEI began in the late 1980's, and accelerated between 1998 and 2005 [*Gardner and Sharp*, 2007]. Since 2005, even more rapid increases in summer air temperature have resulted in higher rates of summer melt and more negative climatic mass balances on the region's glaciers [*Sharp et al*., 2011; *Gascon et al*., 2013]. Significant summer melt now occurs at almost all elevations on these glaciers. In the accumulation area, much of the resulting meltwater percolates into the surface firn layer and refreezes. This process results in the formation of infiltration ice [*Cogley et al.*, 2011], and has the potential to buffer the relationship between increasing melt production and glacier runoff. It may therefore delay the response of eustatic sea level to the observed climate warming [*Harper et al*., 2012].

In the percolation zone, the downward transport of meltwater within the firn typically occurs by heterogeneous infiltration or piping, where refreezing results in small-scale pipe infills and the formation of ice lenses [e.g. *Pfeffer and Humphrey*, 1996; 1998]. In the wet snow zone, thin ice layers are formed when

[2] A version of this chapter has been published as Gascon, G., M. Sharp, D. Burgess, P. Bezeau, and A. Bush (2013), Changes accumulation-area firn stratigraphy and meltwater flow during a period of climate warming: Devon Ice Cap, Nunavut, Canada, *Journal of Geophysical Research: Earth Surface*, doi: 10.1002-2013JF002838.

the snow surface is wetted, and percolating meltwater refreezes within the firn [*Cogley et al.*, 2011]. At lower elevations in the accumulation area, where summer mean air temperature is warmer, superimposed ice forms by refreezing of water on or above the current summer surface [*Cogley et al.*, 2011]. The term glacier ice is restricted to ice formed by firn compaction.

The distribution, abundance and thickness of ice layers within the firn layer of ice sheets and ice caps are often used as indicators of the intensity of surface melt in past summer seasons [*Koerner*, 1977]. Ice layer-derived melt records from cores recovered from ice caps in the QEI show that melt rates in the last 25 years have been the highest in the last two thousand years [*Fisher et al.*, 2012]. Latent heat released during the refreezing of meltwater percolating into firn has contributed to raising firn temperatures by as much as 10°C on Penny Ice Cap (Baffin Island) since the mid 1990's [*Zdanowicz et al*., 2012], and by as much as 3.8 °C on Devon Ice Cap since 2004 [*Bezeau et al*., 2013]. However, very little is known about exactly how freezing of percolating meltwater will fill the available pore volume in firn as climate warms, or how the pattern of pore filling will influence the relationship between surface melt and runoff.

A scenario in which the presence of a thick ice layer within firn impedes the vertical flow of meltwater and promotes lateral flow along its surface was first proposed by *Müller* [1962], and later simulated by *Pfeffer et al.* [1991]. This scenario is consistent with recent observations from the accumulation area of the Devon Ice Cap, where comparisons of density profiles of firn cores drilled in 2004 and 2012 showed formation of thick ice layers close to the ice cap surface and increases of 13-80% in the densification rate of the top 2.5 m of the firn column over the intervening time period [*Bezeau et al.*, 2013]. These changes accompanied the increase in surface melt and refreezing since 2005, and resulted in the ~150 m a.s.l. migration of the superimposed ice zone to higher elevation between 2004 and 2012. As *Bezeau et al.'s* study was based on shallow ice cores drilled in 2004 and 2012, it provides little insight into how the stratigraphy of the firn body as a whole developed over the intervening eight year period, or into how changes in firn stratigraphy were related to evolving patterns of water flow and storage within the firn layer. Here we address these issues using high resolution, multi-year ground-penetrating radar (GPR) measurements that are spatially continuous and extend across the entire elevation range of the firn body. This approach allows us to document the spatio-temporal pattern of changes in firn stratigraphy, and provides new insights into the processes that control them.

We use data from 500 MHz GPR/GPS surveys conducted annually from 2007 to 2012 to document the evolution of the stratigraphy of the firn layer of Devon Ice Cap. Our uniquely high-resolution dataset allows us to track the migration of the boundaries between the ice cap's major facies zones (superimposed ice (SI), wet snow, and percolation zones) over time with an accuracy on the order of meters, describe the annual progression of ice layer growth, and explore the two-way interactions between the evolving firn stratigraphy and patterns of meltwater storage and drainage.

3. 2 Data collection

3.2.1 Field site

The Devon Ice Cap is located on the eastern part of Devon Island, Nunavut, Canada, has an area of ~14,000 km^2 [*Dowdeswell et al*., 2004], and a maximum elevation of ~1900 m a.s.l. The elevation of the surveyed transect at the southern margin of the ice cap is ~500 m a.s.l. The average density of the winter snowpack is ~300 kg m^{-3}, and the annual accumulation rate is ~0.23 m w.e. a^{-1} [*Koerner*, 2005; *Colgan and Sharp*, 2008]. Glaciological facies zones on the ice cap include glacier ice, superimposed ice, wet snow and percolation zones. A quasi-dry snow zone in which melt occurred in some, but not all years, was historically present [*Koerner*, 1977], but has disappeared as surface melting has spread to all elevations on the ice cap as a result of recent summer warming [*Wolken et al.*, 2009].

Multiple field campaigns have been conducted on the ice cap since 2004 as part of efforts to calibrate and validate (Cal/Val) the radar altimeter onboard the European Space Agency's CryoSat-2 satellite. These campaigns focused on the "Cryosat Line", a 48-km transect running from 1800 m a.s.l. to 500 m a.s.l. on the south side of the ice cap. The equilibrium line altitude (ELA) determined from annual mass balance surveys along the Cryosat Line was 1145 m a.s.l. in 2005, but it increased to 1482 m a.s.l. in 2007 and 1585 m a.s.l. in 2011. In support of the Cal/Val effort, research has focused on quantifying and understanding the causes of ice cap surface elevation changes [e.g. *Burgess and Sharp*, 2008; *Colgan et al.*, 2008] and on validating the accuracy of the satellite elevation measurements. The Cryosat line was visited at least once per year from 2007-2012, typically in April or May. Annual spring field campaigns involved collection of measurements from continuously logging Automatic Weather Stations and temperature sensors, mass balance stakes, firn cores, snow pits, GPR surveys, and both static and kinematic GPS surveys.

The period of measurements reported in this study (2004-2012) was the warmest period over the ice cap in the last 60 years (Figure 3-1a), and summer (JJA) mean air temperatures increased by 5˚C over this time interval (Figure 3-1b). Previous work has quantified the changes in surface energy balance that have accompanied the recent summer warming and linked them to changes in the Arctic atmospheric circulation [*Gascon et al*., 2013], and used shallow ice core measurements to evaluate the contribution of accelerated firn densification to measured rates of surface elevation change [*Bezeau et al.*, 2013].

3.2.2 GPR transect surveys

The CryoSat line was surveyed every April/May between 2007 and 2012 using a 500 MHz Noggin GPR instrument from Sensors&Software Inc. GPR surveys were conducted along a 40-km portion of the "Cryosat Line", from Site 1 (1800 m a.s.l.) to just south of Site 3 (1000 m a.s.l.), that covers all major snow/firn facies zones on the ice cap (Figure 3-2). Data collected in 2008 were disregarded due to instrument malfunction. GPR survey results for each year show the structure of the end-of-winter snowpack and of the upper part of the underlying firn as it was at the end of the previous summer. The radar's receiving time window was set to 70 ns in 2007, and 134 ns in subsequent years. A time window of at least 70 ns allowed us to obtain information for the first 8 m below the snow surface. As firn cores were used to validate interpretations of each GPR profile, we believe that differences in ice layer thicknesses that were attributable to the use of different receiving time windows in different years would have been obvious from comparisons between layer thicknesses derived from cores and interpretation of GPR data. Every trace consisted of an average of four measurements, except in 2009 when every recorded trace was an average of 256 measurements. Traces were recorded every 1 s in 2010, 2011 and 2012, and every 5 s in 2007 and 2009. The number of points per trace was set to 650 in all years, leading to a sample interval of no greater than 0.21 ns.

GPR positioning was determined from concurrent differential kinematic GPS measurements. A Leica Geosystems series 500 dual frequency GPS system was used between 2007 and 2011, and a Leica Viva GS15/CS15 Bluetooth system was used in 2012. The GPS antenna was mounted on a Komatiq sled, and the GPR was installed on a separate 3-mm thick plastic bottomed sled towed behind the Komatiq. The entire system was towed by a snowmobile at a speed of 5-7 km h^{-1}. The GPS data were post-processed with Leica Geo Office software using data from GPS reference stations located within 6 km of the mobile GPS system. Base station data were post-processed to an accuracy of < 5 mm in the vertical using the Online Global GPS Precise-Point Positioning (PPP, http://www.geod.nrcan.gc.ca/online_data_e.php) service operated by Natural Resources Canada. Using the corrected base station coordinates, the kinematic rover data were processed to an accuracy of 20-60 mm in z, and 5 mm in x-y.

3.2.3 GPR grid surveys

Although we tried to precisely repeat the track along which annual GPR measurements were made, local navigation errors of up to 65 m across track did occur in some years. Thus, it is possible that some fraction of the GPR-measured changes in the firn stratigraphy may reflect local spatial variability, rather than temporal changes alone. To determine whether this was a significant problem, we conducted four grid-based GPR surveys centered along the main transect to quantify the degree of horizontal variability in the firn and ice layer stratigraphy at each location in 2012. This was done using the same 500 Mhz GPR used for the along-transect surveys. The surveyed grids measured 100 m perpendicular to the transect by 200 m parallel to the transect, and were centered around HB 4-7 (percolation zone), HB 9-1 (wet snow zone), HB 13-7 (SI zone), and Site 2 (SI zone) (see Figure 3-2). Spacing between the surveyed lines was 50 m for lines oriented perpendicular to the transect, and 10 m for lines aligned parallel to the transect, for a total of five 100-m lines and 10 200-m lines, respectively. As with the along track surveys, GPR positioning was determined from concurrent differential kinematic GPS measurements. This allowed us to compare the relative magnitudes of horizontal and temporal variability in firn stratigraphy at each site, and to be confident that our repeat surveys were largely measuring temporal variability.

3.2.4 Firn core stratigraphy and density

To assist with the interpretation of the GPR return signals, shallow firn cores were collected from 10 sites in the accumulation area between MB 5-8 and MB 15-9 (Figure 3-2). As detailed analyses of these ice cores have been reported by *Bezeau et al*. [2013], only a brief description of the dataset is provided here. Cores were drilled using a Kovacs MK II ice coring drill with an internal barrel diameter of 9 cm. Cores were recovered from all sites in 2006, 2011 and 2012, and every other site in 2008 and 2009. No cores were drilled in 2007 or 2010. A total of 36 firn cores were analyzed. Core lengths ranged from 2.60 m to 16.02 m (Table 3-1). From 2006-2011, cores were logged on site using a combination of direct visual observations complemented by photography taken with a visible spectrum digital camera. Cores drilled in 2012 were logged on site using infrared photography with a modified Fuji FinePix S9000 digital camera [*Bezeau et al.*, 2013]. Constituents of the cores were classified as either firn or ice based on differences in bubble content, density, and crystal structure. For all years, we derived firn core density profiles by dividing the mass of each firn core segment by its volume. Core segments were 0.04-0.25 m in length, and consisted of the relatively homogeneous material between density transitions along the core. Errors associated with the measurement of each segment's weight and length were estimated to be 0.02 kg and 0.01 m, respectively, leading to an average density measurement error of 40 kg m^{-3}. Since firn and ice densities in the accumulation zone of the Devon Ice Cap range between 450 and 880 kg m^{-3}, this represents an error of 5-9%.

3.3 Methods

3.3.1 GPR data processing

GPR data were processed using the EKKO_View Deluxe and EKKO_View 2 software packages from Sensors&Software in such a way as to easily identify and differentiate internal reflecting horizons (IRH) associated with boundaries between ice and firn layers in all facies zones. On the Devon Ice Cap, the density of ice layers is internally homogeneous, while that of firn tends to fluctuate rapidly over short distances in the vertical. Firn and ice thus appear differently on GPR profiles due to their distinctive densities and patterns of internal density variability.

GPR data were first cleaned of static measurements that were collected while the instrument was not moving. Initial processing included application of a Dewow filter, time-zero correction, background subtraction, and time-varying gain, and correction for surface topography using GPS data. Specific processing options were also applied for three different types of analysis, as described below.

1. GPR processing was designed to ensure that ice and firn layers were identifiable throughout the surveyed transect. After careful investigation of different processing approaches, Spreading and Exponential Calibrated Compensation (SEC2) gain with an attenuation of 1, start gain ranging between 0.75 and 1.25, and a maximum gain set to 100 was applied to the data. This highlighted moderate and strong reflections from within the firn, without amplifying weak reflections from within ice layers with more uniform density. Regions of ice remained relatively homogeneous-looking within the plotted GPR profiles and internal reflections had low amplitudes compared to reflections from within firn and at firn-ice boundaries. With the chosen color palette, this caused ice layers to show as white in the screen display, while firn with internally varying densities and well-defined ice-firn boundary transitions showed as purple and blue throughout the surveyed transect.

2. To successfully validate the interpretation of the GPR-inferred firn stratigraphy through comparison with firn core stratigraphy, the GPR data had to be processed in a way that allowed sharp separation between regions with multiple internal reflecting horizons (i.e. firn) and regions with few or none (i.e. ice, which is internally homogeneous relative to firn). To achieve this, a temporal Hilbert transform envelope using a filter width of 4.0 ns was applied to the GPR data. The envelope attribute makes it possible to display zones with little internal density variation (high homogeneity) as single thick layers since it omits zero amplitude transitions.

3. The 2012 GPR data collected in gridded patterns required a higher degree of processing to facilitate interpolation between the lines. These data were processed using EKKO_Mapper software from Sensors&Software to facilitate horizontal slice image extraction. In addition to the initial processing applied to all GPR data, a temporal Hilbert transform envelope, migration, and amplitude equalization gain (attenuation = 1, start gain = 0, maximum gain = 100) were applied. Migration facilitates interpretation of slice images by collapsing

hyperbolic reflections to a point. The amplitude equalization gain compensated the weaker signals from greater depths while processing slice images.

3.3.2 GPR depth and velocity calibration

In order to accurately map the geometries of the major ice bodies within the firn and measure their changes over time, it is critical to determine the absolute depths of IRHs. For this, firn stratigraphies derived from cores drilled to 8 m depth at HB 9-1, HB 13-7 and Site 2 in 2012 were used for GPR velocity calibration, and for validation of the stratigraphic interpretation of the radar profiles. These three sites were chosen specifically because their firn core stratigraphies included sharp vertical transitions between firn and ice, a characteristic ideal for GPR velocity and depth calibration. High resolution GPR surveys were conducted directly above the borehole sites prior to drilling to ensure comparability of the GPR and firn core data. The GPR data were processed as described in Section 3.3.1. The GPR-inferred firn stratigraphies at each of the three sites were mapped by identifying IRHs associated with firn-ice and ice-firn transition boundaries (Figure 3-3a). The depths of these IRHs at each site were then determined by comparison with the depths of the ice and firn layers derived from core stratigraphy and density profiles at the same site (Figure 3-3b). Wave velocity was determined by associating each major IRH with its corresponding depth as measured from the firn core data (Figure 3-3c). Wave velocity estimates were determined in firn with densities ranging from 475 to 650 kg m^{-3}, and varied between 0.225 and 0.245 m ns^{-1}. A value of 0.23 m ns^{-1} was chosen for the mean wave velocity for the 0 to 8 m depth range because it produced the smallest IRH depth error. By comparison, velocities calculated from measured densities using the theoretical relationship provided by *Kovacs et al.* [1995] averaged 0.206 nm s^{-1}. Using a velocity of 0.23 m ns^{-1}, the estimated error in the depth of the different IRHs associated with ice and firn layer boundaries ranged from 0.10 m to 0.20 m and 0.10 m to 0.35 m respectively.

3.4 Results

3.4.1 GPR characteristics of firn facies

As elevation decreases with increasing distance along the transect, the amount of surface melt produced in summer likely increases, leading to the presence of different snow/firn facies at different elevations. Each snow/firn facies shows specific structures in the GPR profiles (Figure 3-4), which reflect the different processes involved in their formation. This allows us to track changes in facies distribution over the study period (see Section 4.3). Analysis of the GPR survey data from each grid site provides additional detailed information about the local characteristics of the firn stratigraphy within each facies zone. Definitions of the percolation, wet snow, superimposed ice, and glacier ice zones follow *Cogley et al.* [2011].

Discontinuous ice layers, ice pipes and ice lenses define the presence of infiltration ice in the percolation zone. Such ice features are typically localized and of small scale (< 0.15 m thick), and can be identified in ice core stratigraphy (Figure 3-5a). The stratigraphy of the mixture of firn and ice in the percolation area is highly heterogeneous due to the presence of these discontinuous ice features. As a result, there are many internal radar reflectors, and GPR profiles fail to capture small and discontinuous ice elements. In the GPR profiles, the percolation zone is identified as a region where continuous IRHs are absent and there is large small-scale variability (Figures 3-4, 3-5a). The noisy radar signature reflects the absence of continuous ice layers, and the large number of snow and firn layers of different density, the boundaries between which act as discrete scattering surfaces. The lower boundary of the percolation zone is called the wet-snow line (1640 m a.s.l. in 2012), and it marks the transition to the wet snow zone at lower elevations.

The wet snow zone (or lower percolation zone) is defined as the region in which the temperature of the whole of the previous winter's snowpack is raised to the melting point and becomes isothermal during the melt season. Here, some meltwater percolates through the winter snowpack and into the underlying firn, where it refreezes, creating an ice layer embedded within the firn. Heterogeneous percolation and refreezing lead to stratigraphic discontinuities and the presence of residual firn within, and between, major ice layers. In ice core stratigraphy, the wet snow zone is identified by the presence of discontinuous ice layers 0.5-1.5 m thick with firn above and below them (Figure 3-5b). On GPR profiles, the wet snow zone is characterized by the presence of thick layers of generally low radar reflectivity at depths between 1 and 3 m which represent homogeneous ice, with some residual firn embedded within it. Regions of high radar reflectivity above and below the ice layers represent heterogeneous firn of varying density (Figures 3-4, 3-5b). The lower boundary of the wet snow zone is called the snow/firn line (1520 m a.s.l. in 2012), and coincides with the upper boundary of the superimposed ice zone. This is the boundary between firn and ice on the ice cap surface at the end of the melt season.

The superimposed ice zone is located at lower elevations than the wet snow zone, where air temperature is warmer and more surface meltwater is produced. It is the region where the previous winter's snow pack is completely melted, but some residual meltwater refreezes on top of the previous year's end-of-summer surface to form a layer of accumulation in the form of superimposed ice. Ice cores from sites HB 13-7 and Site 2 clearly show these firn/ice layering characteristics and are used as a reference to identify the superimposed ice zone on GPR profiles (Figure 3-5c-d). On GPR profiles, the superimposed ice zone is defined by a zone of low reflectivity (homogeneous ice layer) that occurs just below the winter snowpack, with evidence of internal layering associated with the uneven refreezing of percolated meltwater (Figures 3-4, 3-5c-d). *Sylvestre et al.* [2013] pointed out that a well-defined ice layer formed over the Belcher Glacier on the north side of the Devon Ice cap during (or at the end of) the warm summer of 2005. Using this information, a layer identified as L2005 on GPR profiles defines the IRH associated with the basal boundary of the 2005 ice layer (Figure 3-5c-d).

The lower boundary of the SI zone coincides with the equilibrium line, below which glacier ice is exposed at the surface in the ablation area in summer. On GPR profiles, the upper boundary of the glacier ice zone is identified by the upwards deflection of IRH's towards the surface. It is present in the lower part of the survey area, and is characterized by faint IRH's that show the relative homogeneity of the glacier ice (Figure 3-6).

3.4.2 Horizontal spatial variability

In order to properly identify the differences between the GPR profiles measured between 2007 and 2012, we must first assess the local spatial variability in firn stratigraphy. If this is large, then small changes in transect location between years could alone account for the differences between the GPR profiles. If local variability is small, however, then differences between the GPR profiles can be attributed to temporal changes associated with the observed increases in air temperature and surface melt. Here, we use the variability in the thickness of the major ice layers in the accumulation area of the ice cap to assess the degree of local spatial variability in the stratigraphy of the firn layer. The average thickness of the major ice layers in the vicinity of HB 9-1, HB 13-7 and Site 2 was determined by sampling the ice thickness every 10 m along each of the 15 lines surveyed in each gridded GPR survey, that is along five 100-m lines, and ten 200-m lines. This provided information on the horizontal variability of the ice layer thicknesses over an area of 0.02 km^2 at each site (Table 3-2). The standard deviations of the ice layer thicknesses range from 0.11 m at HB 9-1, to 0.16 m at HB 13-7 and 0.18 m at Site 2. Relative to the average thicknesses of the ice layers, these values represent spatial variability of 15, 2 and 4%, respectively. The higher percentage variability at HB 9-1 is associated with a thinner ice layer containing more residual firn than the layers at the other sites (Figure 3-5b). In contrast, HB 13-7 and Site 2 are located in the SI zone, where multi-year refreezing of percolating meltwater filled almost all the pore volume, resulting in thicker and more continuous ice layers (Figure 3-5c-d). The GPR grid surveys show relatively little lateral variability in ice layer thickness. The standard deviations of the thickness of the main ice layers at the three sites (0.11-0.18 m) are very small compared to the changes in ice layer thicknesses observed between 2007 and 2012 (0.5-4.5 m, see Section 4.3). Positioning error of the repeated GPR surveys (< 65 m) is therefore highly unlikely to account for the observed changes in firn stratigraphy since ice layers in the surveyed portion of the accumulation area of the ice cap are continuous, and display little spatial variation in thickness over a distance of 100-200 m.

3.4.3 2007-2012 migration of glaciological facies zones

GPR surveys were used to track the changes in the position of the upper boundaries of the superimposed ice and wet snow zones between 2007 and 2012 (Figure 3-6). Since the most substantial changes occurred in the region between km 5.8 and 15.9 (sites MB 5-8 and MB 15-9), enlarged GPR profiles for that region are presented in Figure 3-7. The ice motion over the surveyed area of the Devon Ice Cap is on the order of 5-10 m yr^{-1} [*van Wychen et al.*, 2012]. This represents a displacement of 25-50 m in the position of specific parcels of ice between 2007 and 2012. As this distance is small compared to the distance over which firn facies boundaries migrated during the same period of time (4.5-14.5 km, see below), we conclude that ice motion is unlikely to account for the changes in facies distribution observed over the study period. Since ice motion would advect the upper limits of the facies zones downglacier and the results presented below report them moving upglacier, we could in fact be slightly underestimating their maximum upglacier displacements.

As a reference for the depth at which the first signature of the major melt episode on the Devon Ice Cap is captured by the GPR, the 2005 ice layer (L2005) is identified on Figures 3-6a, 3-7 and 3-8a. Spring 2007 GPR data have a gap between km 18 and km 20 that unfortunately prevents us from knowing the exact location of the transition between the thick ice layer observed below km 20 and the L2005 IRH observed above km 18. In spring 2007, the upper limit of the SI zone was located around km 27 (1220 m a.s.l.), and that of the wet snow zone was around km 12.5 (1520 m a.s.l.) (Figures 3-6a, 3-7a). By 2009, the upper boundaries of the SI and wet snow zones had migrated to km 18 (Site 2, 1400 m a.s.l.) and km 9.5 (1600 m a.s.l.), respectively. Thicker and more sharply-defined ice layers in the wet snow zone between km 12.5 and 18 in 2009 suggest significant thickening of the ice body between 2007 and 2009. The ice layer that formed during the 2005 summer appears to have been largely impermeable to percolating water, explaining why it accreted upwards between 2007 and 2009. The upper boundaries of the SI and wet snow zones continued to migrate upglacier in springs 2010, 2011 and 2012 (Figures 3-6 c-e, 3-7c-e), to reach km 12.5 (1520 m a.s.l.) and just below km 8 (1640 m a.s.l.), respectively, by 2012. After spring 2010, a second thick ice layer formed above the L2005 layer in the wet snow zone between km 8 and km 11.7 (L2010). Between springs 2007 and 2012, thickening of the ice layers ranged from 0.5 m near km 8-9, to > 4.5 m below km 13.5. Relative to its position in spring 2007, the upper limit of the SI zone had migrated 14.5 km upglacier, and 300 m higher in elevation by 2012. Over the same time period, the upper limit of the wet snow zone migrated 4.5 km upglacier and 120 m higher in elevation.

3.4.4 Ice layer evolution

The observed changes in firn stratigraphy occurred primarily above the L2005 ice layer. The behavior of percolating meltwater as it reached the L2005 layer was investigated further by differencing the annual GPR sections to map the evolution of the ice content of the firn between 2007 and 2012 in the region between MB 5-8 and MB 15-9 (Figure 3-8). While vertical accretion of ice above the L2005 layer was the dominant process, some heterogeneous vertical percolation did occur to depths below the L2005 layer. Below km 12.5, multiple ice layers formed in the firn and each thickened over time, especially over small ridges located around km 13 and km 14.5 (Figure 3-8). The results suggest that water percolated to depths of 5-6 m, particularly early in the study period. Once all residual firn was eliminated, however, the ice layers merged into a single ice body, as shown by the decline in formation of new ice layers around km 13 and km 14.5 in springs 2011 and 2012. By this time, the main ice body was thick enough to impede vertical percolation and caused infilling of depressions in the upper surface of the ice layer by vertical ice accretion. Above km 12.5, however, the main ice body was not thick enough to impede vertical percolation significantly, as shown by the continued formation of new, smaller ice lenses and layers below it (Figure 3-8). The region of formation of such deep ice layers migrated progressively further upglacier in each spring, suggesting that at lower elevations percolating meltwater was being intercepted by an impermeable ice layer (Figure 3-8). Where the surface slope of the ice layers was either very low (< 1˚) or directed upglacier, percolating meltwater became ponded above the ice layers and froze at the end of the melt season. If the surface slope of the ice layers was larger (1-2.5˚) or directed downglacier, however, meltwater flowed and refroze laterally above them (Figure 3-8). In either case, firn below the main ice layer was cut-off from percolating water, creating a region with significant available pore space that was isolated beneath a thick, impermeable ice body. Thus, by hydrologically isolating the deeper parts of the firn aquifer from surface recharge, the formation of thick infiltration ice within the firn appears to have reduced the internal water storage capacity of the ice cap.

3.5 Discussion

The firn stratigraphy changes observed on the Devon Ice Cap were a response to a warming summer climate. *Gascon et al.* [2013] calculated that the surface melt rate at 1400 m a.s.l. on the Devon Ice Cap increased from 0.74 to 1.33 m w.e. a^{-1} between 2007 and 2010. As these changes are much larger than observed inter-annual variability in the water equivalent of the end-of-winter snowpack of ~0.23 m w.e. a^{-1} [*Koerner*, 2005; *Colgan and Sharp*, 2008], we associate the increased ice content of the firn with increased summer melt, rather than with a decrease in accumulation rate. The increase in surface meltwater production associated with the recent warming over the Devon Ice Cap and the resulting increase in percolation and refreezing of meltwater modified the stratigraphy of the firn significantly over a horizontal distance of nearly 30 km between springs

2007 and 2012 (Figures 3-6 and 3-7). The upper limit of the superimposed ice zone migrated from ~1430 m a.s.l. in spring 2007 to ~1520 m a.s.l. in spring 2012, a horizontal displacement of ~14.5 km. The upper limit of the superimposed ice zone in 2012 derived from our higher resolution data (~1520 m a.s.l.) is slightly lower than that reported by *Bezeau et al.* [2013] (~1550 m a.s.l.) on the basis of measurements on firn cores. Between 2007 and 2012, the upper limit of the wet snow zone migrated from ~1520 m a.s.l. to ~1640 m a.s.l., a horizontal displacement of ~4.5 km. The upper-boundary of the SI zone can migrate to higher elevations when infiltration ice in the wet-snow zone becomes so thick that water cannot penetrate it and refreezing therefore occurs on top of it. The presence of residual firn within and beneath the upper parts of the SI zone reflects temporal changes and variability in summer melt intensity, as well as the heterogeneity of meltwater percolation into firn (Figure 3-4). Strong summer melt tends to reduce the occurrence of residual firn as more meltwater percolates and refreezes in the subsurface of the ice cap. GPR surveys showed formation of new ice layers that eventually reached 0.5 to 4.5 m in thickness by spring 2012. This resulted in the increase of the mean density of the upper 2.8 m of firn cores by 17-35% between spring 2007 and spring 2012 as reported by *Bezeau et al.* [2013].

The pattern of ice layer formation illustrated in Figure 3-8 suggests that, as the ice body became thicker, less surface meltwater was able to percolate through it. Thus, increasing the ice content of the firn progressively reduced its permeability, eventually blocking or reducing vertical percolation of meltwater, and enhancing upwards accretion of ice. The initial thick ice layer (L2005) is thought to have been largely impermeable to percolating melt water, forcing meltwater to either pond above it or flow horizontally across it through the firn rather than percolate to greater depths. Increased refreezing of percolating meltwater contributed to the rapid infilling of available pore volume above L2005 after spring 2007 (Figure 3-7). This process was responsible for the persistent upwards accretion of ice in the wet snow zone, and the reduction in the number of IRHs associated with residual firn within the main ice body in the SI zone.

Small hills and troughs can be identified along the surveyed profiles (Figure 3-7). Such features are no more than 5 m high, but appear very significant because of the large vertical exaggeration. Nevertheless, this topography had an important influence on how the pore volume became filled by ice. Concave upwards regions of the ice cap surface trapped blowing snow, leading to spatial variability in annual snow accumulation of ~0.1 m w.e. between hills and troughs [*Bezeau et al.*, 2013]. Similar spatial variability of snow accumulation has been observed on Greenland [*Miège et al.*, 2013]. On the Devon Ice Cap, meltwater was apparently able to percolate downward more easily at the tops of the small hills, where snow accumulation was reduced, while dense wind-packed snow formed in areas of deposition. Ice was thus more easily accreted in these regions. As the ice layer in crest regions became progressively thicker, infiltrating meltwater was forced to flow laterally into depressions in the ice layer surface, where it pooled and then refroze at the end of the summer, progressively filling the firn above the depressions with infiltration ice (Figure 3-8c-d). Rolling surface topography was thus associated with large-scale heterogeneity in meltwater infiltration, which caused superimposed ice to form at least 3 years sooner at the tops of the hills than in intervening depressions (Figure 3-7).

Meltwater retention and refreezing in firn delay the contribution of increasing melt to glacier runoff [*Harper et al*., 2012]. *Humphrey et al.* [2012] tracked the thermal signature of meltwater infiltration in the percolation area of Greenland between 2007 and 2009 and found that some areas at depth became fully saturated, suggesting some lateral flow of meltwater downglacier under low hydraulic gradients. As the average surface slope of the percolation area of Greenland is < 0.5˚, lateral water flow is expected to be very slow and heterogeneous, and the primary signature of refreezing would be small-scale piping. As the average surface slope of the percolation area of the Devon Ice Cap is 2˚, more lateral flow of meltwater is to be expected there. Although thin ice layers resulting from refreezing of percolating meltwater have been observed in the percolation area of western Greenland using GPR surveys [*Brown et al.*, 2011], the depth of meltwater penetration exceeded 10 m (but has yet to be fully constrained) [*Humphrey et al.*, 2012]. In contrast, on the Devon Ice Cap, rapid formation of a thick ice body limited deep percolation of meltwater below the newly-formed ice layers. Ice layer formation suggests that a large fraction of the melt water produced since 2007 has been retained within the ice cap.

Bezeau et al. [2013] calculated that the mean rate of thickness change associated with firn densification at 1400 m a.s.l. (Site 2) between 2004 and 2012 was -0.103 m a^{-1}. Assuming that this rate is constant over time and that the density of ice is 850 kg m^{-3}, this is equivalent to forming 0.09 m w.e. of infiltration ice per year. Using the surface melt rate calculated by *Gascon et al.* [2013], this implies that the fraction of melt water produced that was retained within the firn decreased from 12% in 2007, to 7% in 2010. This suggests that the thick ice layer became essentially impermeable to percolating meltwater by 2012. Indeed, the thickness of the ice layer around Site 2 (Figure 3-6, 18 km) has not changed significantly since the spring 2011 survey. This leads us to believe that surface meltwater is now forced to run off from the accumulation area of the ice cap. However, the presence in this region of numerous lakes that drain during the summer suggests a more complicated hydrologic system that requires further study.

Given the projected increase in summer air temperatures over the Arctic [*Meehl et al.*, 2012], we believe that the combination of high surface melt, relatively steep slopes, and rapid firn densification will reduce vertical percolation of meltwater at even higher elevations on the Devon Ice Cap. The Devon Ice Cap receives little precipitation during the summer months due to the presence of persistent high pressure systems over the Canadian Arctic that result in clear-sky conditions [*Gascon et al.*, 2013]. North American Regional Reanalysis (NARR) data suggest that rain events (< 5 mm) currently occur 4-5 times per season in the ablation area, but that only 2 rain events occurred at higher elevations in the last

10 years. A warming climate may increase the occurrence of rain events, but given the generally dry conditions over the Devon Ice Cap, rain-on-ice events are not likely to produce sufficient energy to penetrate the thick ice layer and introduce water to the firn below. Instead, rain will likely refreeze within the winter snowpack if it falls at the beginning of the summer, or run off if it falls at the end.

The formation of quasi-impermeable ice layers that would restrict vertical flow of meltwater and enhance surface runoff was first suggested by *Müller* [1962], but has never been observed until now. However, continuous ice layers have not yet been observed above 1640 m a.s.l. on Devon Ice Cap. This suggests that, at such high elevations, where surface melt rates and surface gradients are lower, deep meltwater percolation could still take place. Some (or all) of the meltwater produced will eventually freeze and warm the firn through latent heat release. Firn warming will also be enhanced by the direct effect of atmospheric warming [*Bezeau et al.*, 2013], and the firn temperature may eventually approach the pressure melting point. If this point can be reached without the pore volume of the firn being completely filled by ice, meltwater that eventually flows horizontally downglacier may become trapped beneath the continuous ice layers of the wet snow and superimposed ice zones, which eventually merge downglacier with underlying glacier ice. This might, in due course, result in the buildup of a liquid water reservoir below the ice cap surface, as has recently been observed on southern parts of the Greenland Ice Sheet [*Forster et al.*, 2012].

3.6 Conclusion

Spatial and temporal changes in the stratigraphy of firn on the Devon Ice Cap, Nunavut, were examined using GPR data collected between 2007 and 2012. These changes were a response to abnormally warm summer temperatures across the ice cap. Data clearly showed rapid densification of the firn, the formation of extensive, continuous ice layers within the firn body, and the spread of more rapid densification and ice layer formation to higher elevations on the ice cap over time.

After the initial period of ice layer formation, much of the ice layer growth occurred by upward vertical accretion above a thick quasi-impermeable ice layer. The rolling topography caused large-scale heterogeneous percolation of surface meltwater. Refreezing was initially concentrated over small ridges. By spring 2011, this caused lateral flow diversion to basins, and caused ponding and refreezing of meltwater in the concave regions. One consequence of this may have been a reduction in the ability of firn to buffer the relationship between surface melt and runoff through storage of water as ice within firn. Indeed, the ice layers significantly reduced vertical percolation of meltwater into deeper parts of the firn, to the point that water retention at 1400 m a.s.l. was $\leq$ 7% by 2010. Ultimately, this process has the potential to trigger a positive feedback at the ice-cap scale, whereby an increase in surface melt and near-surface runoff will occur from sections of the accumulation area where internal refreezing previously absorbed most or all of the annual melt, and thus reduce the surface mass balance of the ice cap. However, continuous ice layers have yet to reach the summit of the ice cap, and it remains a possibility that deep meltwater percolation in this region could result in downslope drainage beneath the ice layers that could lead to refreezing and filling of the buried firn pore volume, or result in the buildup of a firn aquifer.

We showed that thick ice layer formation promoted horizontal runoff on the Devon Ice Cap. Most mass balance models, however, only assume vertical percolation of meltwater [*Reijmer et al.*, 2012]. In the presence of thick, impermeable ice layers, this assumption would lead to an overestimation of refreezing, and an underestimation of surface runoff to the ocean. Our observations thus suggest a need for surface mass balance models to incorporate more sophisticated two or three dimensional treatments of heterogeneous water flow and refreezing within firn than are currently available, and for the collection of long-term field datasets that would allow calibration and validation of those treatments.

Tables

Table 3-1: Description of firn cores drilled between summers 2006 and 2012.

Site	Latitude	Longitude	Elevation m a.s.l. (± 5 m)	Core length (m) 2006	2008	2009	2011	2012
HB 4-7	75° 17' 55.4" N	82° 42' 12.5" W	1743	---	---	---	---	15.53
MB 5-8	75° 16' 42.4" N	82° 42' 54.3" W	1685	2.60	4.43	3.12	3.46	5.58
MB 6-9	75° 16' 07.4" N	82° 43' 16.1" W	1660	2.90	---	---	3.92	5.67
MB 8	75° 15' 31.2" N	82° 43' 37.5" W	1640	2.82	4.98	---	3.76	5.52
HB 9-1	75° 14' 54.5" N	82° 44' 01.1" W	1610	2.80	---	3.10	4.14	16.02
MB 10-3	75° 14' 15.9" N	82° 44' 24.9" W	1575	2.77	4.65	---	4.00	5.65
MB 11-5	75° 13' 41.0" N	82° 44' 45.7" W	1550	2.86	---	---	3.86	5.56
MB 12-6	75° 13' 05.7" N	82° 45' 05.6" W	1515	2.79	---	2.98	2.79	5.42
HB 13-7	75° 12' 31.6" N	82° 45' 27.3" W	1490	2.59	---	---	3.81	15.85
MB 14-8	75° 11' 56.4" N	82° 45' 49.8" W	1460	3.20	---	---	3.90	5.93
MB 15-9	75° 11' 23.2" N	82° 46' 08.2" W	1440	2.46	---	3.05	3.30	5.24
MB 17	75° 10' 43.6" N	82° 46' 29.9" W	1425	---	---	---	---	---
Site 2	75° 09' 39.2" N	82° 47' 10.0" W	1400	---	---	---	---	15.75

Table 3-2: Statistics of the thickness of the main ice layer at HB 9-1, HB 13-7 and Site 2 from spring 2012 GPR grid survey analysis.

Site	Thickness of the ice (m) Min	Max	Average	Standard deviation
HB 9-1	0.45	1.15	0.73	0.11
HB 13-7	3.60	4.20	3.85	0.16
Site 2	5.43	6.23	5.67	0.18

Figures

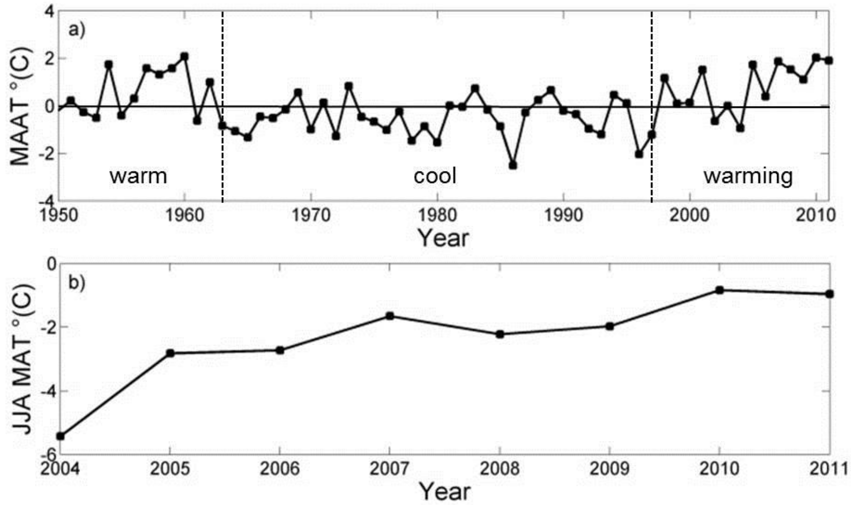

Figure 3-1: a) National Centers for Environmental Prediction (NCEP) 1950-2011 mean annual air temperature (MAAT) anomaly at 700 hPa over the Devon Ice Cap. b) 2004-2011 mean June-July-August (JJA) 2-m air temperature from Site 1 and Site 2 AWS data.

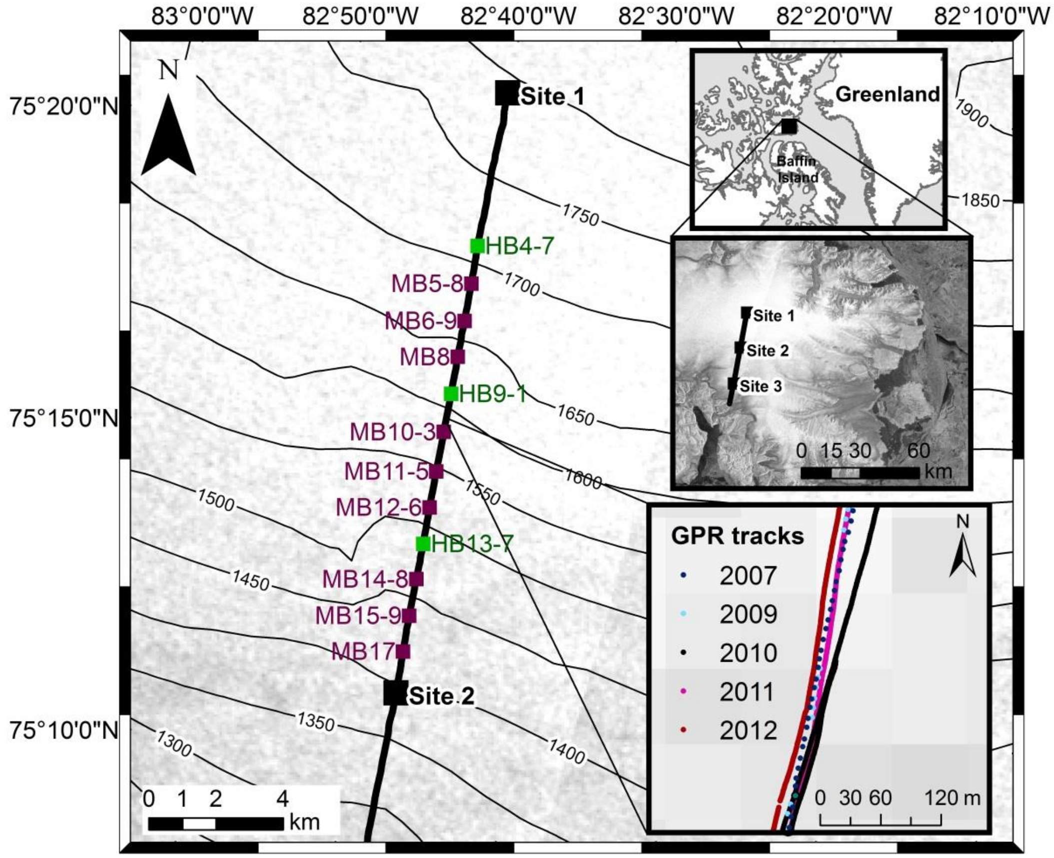

Figure 3-2: Devon Ice Cap field measurement locations. Numbering along the transect line in the main figure represents the firn core sites; their numbers also represents the distances away from Site 1. GPR grids were surveyed at the three HB sites labeled in green and Site 2 in 2012. Firn cores have been drilled at all the labeled sites along the transect. The 2-m air temperatures were measured during the 2006-2011 period with a Beta Therm 100K6A probe mounted on an automated weather station (AWS) at Sites 1 and 2. The bottom right inset shows an example of the distance separating GPR tracks; annual transects were positioned no greater than 65 m apart. Contours are in meters above sea level (m a.s.l.). Average surface slope of the surveyed transect is (2˚) (length 40 km, elevation drop 800 m).

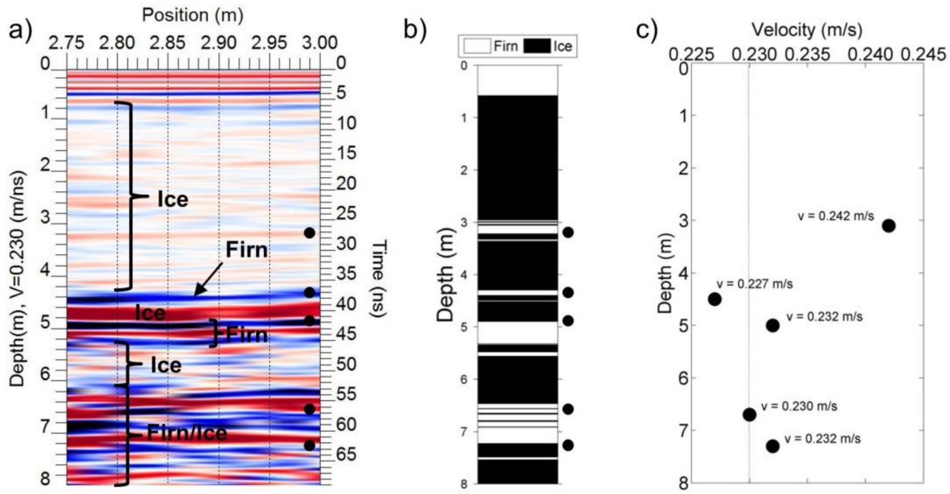

Figure 3-3: GPR wave velocity and depth calibration for Site 2 using ice core stratigraphy. a) GPR profile, where white represents ice layers, and red and blue represents firn of different densities. SEC2 gain and a Hilbert transform envelope were applied to the GPR data. The 0-5 ns section shows the overwinter snowpack. b) Firn core density profile. c) GPR wave velocity at five important firn-ice density transitions of known depths from firn core integrated from the surface down to each reflector. Small dots in a) and b) indicate which density transitions were associated to velocities shown in c).

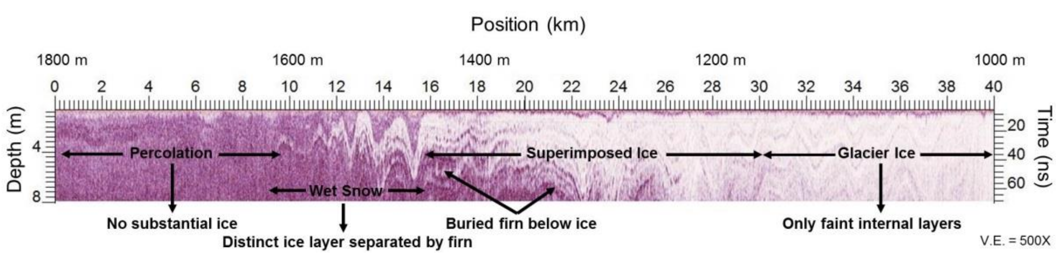

Figure 3-4: A GPR profile of the surveyed transect from 0 km (Site 1) to 40 km (Site 3) for spring 2010. Dewow filter, background subtraction, GPS topography correction and a SEC2 gain were applied to the data. White layers represent ice, and a purple signature represents firn. The different zones are identified along the profile: percolation, wet-snow, superimpose ice, and glacier ice. The x-axis unit is distance (in km) from Site 1, and the surface elevation decreases with increasing horizontal distance. Elevation is in m a.s.l. Average surface slope of the surveyed transect is (2˚) (length 40 km, elevation drop 800 m). Vertical exaggeration (V.E.) is 500X.

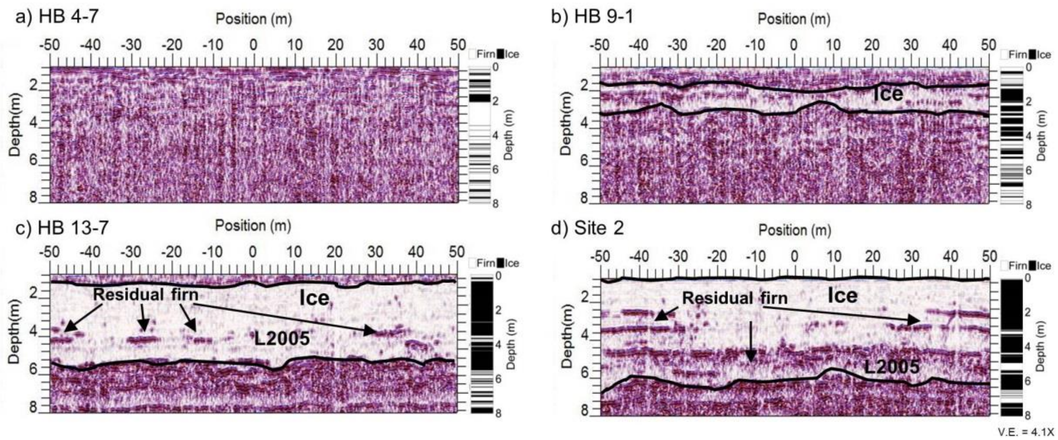

Figure 3-5: A 100-m GPR line across the main transect line, and firn core stratigraphy at each of the four grid sites showing the GPR characteristics of three different snow facies in the accumulation area of the Devon Ice Cap in spring 2012: a) HB 4-7; percolation zone, b)HB 9-1; wet snow zone, c) HB 13-7; SI zone, and d) Site 2; SI zone. Dewow filter, background subtraction, topography correction and a SEC2 gain were applied to the GPR data. L2005 indicates the position of the summer 2005 ice layer, and defines the bottom boundary of the SI region. Vertical exaggeration (V.E.) is 4.1X.

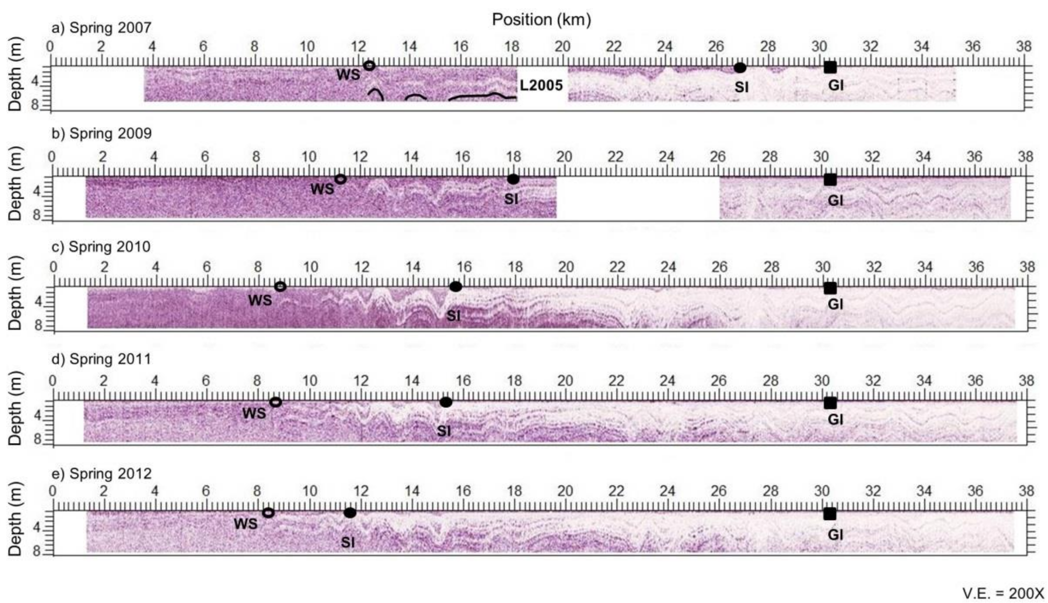

Figure 3-6: Spring 2007-2012 GPR profiles between Site 1 and 2 km above Site 3. Data processed as in Figure 3-4. 2 km and 6.5 km data gaps in springs 2007 and 2009, respectively, were due to the partial GPR failure. Location of the upper-boundary of the wet snow (WS), superimposed ice (SI) and glacier ice (GI) zones are identified. In a), L2005 indicates the position of the summer 2005 ice layer. Vertical exaggeration (V.E.) is 200X.

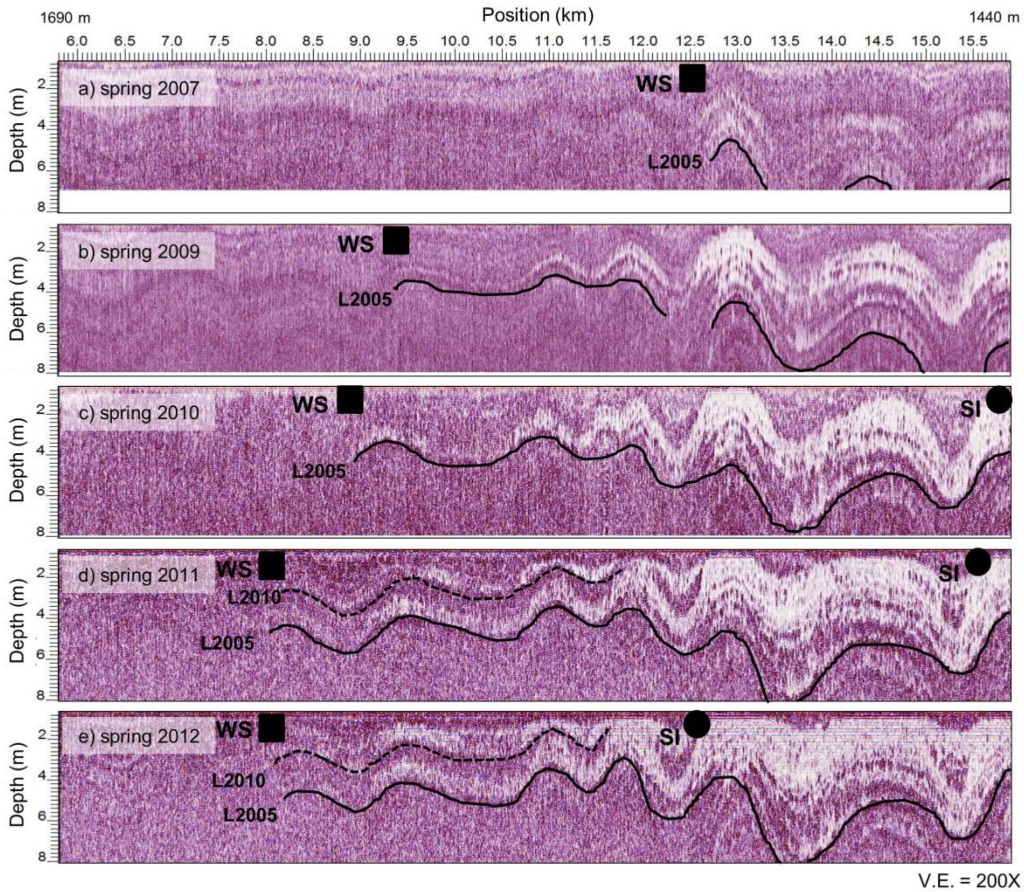

Figure 3-7: Spring 2007-2012 GPR profiles between MB5-8 and MB15-9. Wave-like patterns are associated with rolling topography (and large vertical exaggeration), where concave regions trap snow. Data processed as in Figure 3-4, but enlargement exposes the structure and extent of the ice layer in the wet snow zone in greater detail. Location of the upper-boundary of the wet snow (WS) and superimposed ice (SI) zones are identified. L2005 indicates the position of the summer 2005 ice layer. L2010 indicates the position of the summer 2010 additional ice layer in the wet snow zone. Elevation is in m a.s.l. Average surface surface slope is (2.5˚) (length 10 km, elevation drop 250 m). Vertical exaggeration (V.E.) is 200X. A surface topography profile above the radar images can be found in the online auxiliary material.

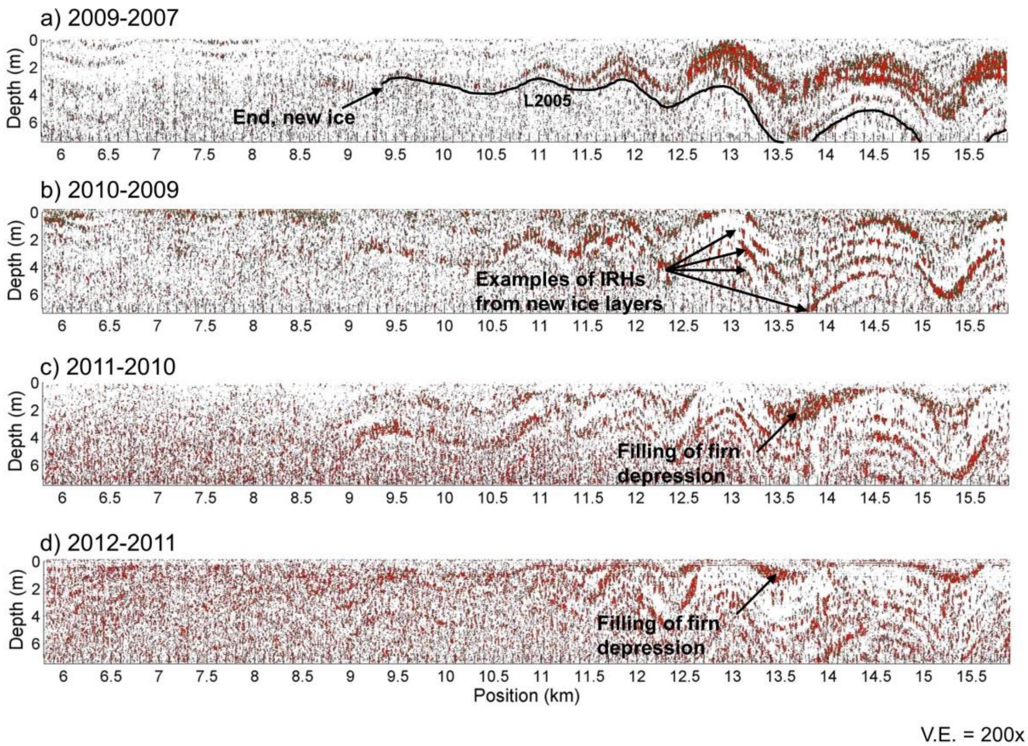

Figure 3-8: Subtraction of the GPR profile of subsequent years to illustrate the evolution of the formation of ice layers in the accumulation area: a) 2009-2007, b) 2010-2009, c) 2011-2010, and d) 2012-2011. In a), L2005 indicates the position of the summer 2005 ice layer. New ice layers are indicated in red. White regions indicate no change in ice content over the given time period. Vertical exaggeration (V.E.) is 200X.

3.7 References

Bezeau, P., M. Sharp, D. Burgess, and G. Gascon (2013), Firn profile changes in response to extreme 21st century melting at Devon Ice Cap, Nunavut, Canada, *J. Glaciol.*, 59(217), 981-991, doi:10.3189/2013JoG12J208.

Brown, J.M., J.T. Harper, W.T. Pfeffer, N.F. Humphrey, and J.H. Bradford (2011), High resolution study of layering within the percolation and soaked facies of the Greenland ice sheet, *Ann. Glaciol.*, (52)59.

Burgess, D.O. and M. Sharp (2008), Recent changes in thickness of the Devon Island ice cap, Canada, *J. Geophys. Res.*, 113, B07204, doi:10.1029/2007JB005238.

Colgan, W., and M. Sharp (2008), Combined oceanic and atmospheric influences on net accumulation on Devon Ice Cap, Nunavut, Canada. *J. Glaciol.*, 54(184), 28–40, doi: 10.3189/ 002214308784409044.

Colgan, W., J. Davis, and M. Sharp (2008), Is the high elevation region of the Devon Island ice cap thickening?, *J. Glaciol.*, 186, 428-436.

Cogley, J. G., R. Hock, L.A. Rasmussen, A. A. Arendt, A. Bauder, R. J. Braithwaite, P. Jansson, G. Kaser, M. Möller, L. Nicholson and M. Zemp (2011), Glossary of Glacier Mass Balance and Related Terms, IHP-VII Technical Documents in Hydrology No. 86, *IACS Contribution*, No. 2, UNESCO-IHP, Paris.

Dowdeswell, J.A., T.J. Benham, M.R. Gorman, D. Burgess, and M.J. Sharp (2004), Form and flow of the Devon Island Ice Cap, Canadian Arctic, *J. Geophys. Res.*, 109, F02002, doi:10.1029/2003JF000095.

Fisher, D., J. Zheng, D. Burgess, C. Zdanowicz, C. Kinnard, M. Sharp, and J. Bourgeois (2012), Recent melt rates of Canadian Arctic ice caps are the highest in four millennia, *Global Planet. Change*, 84–85, 3–7.

Forster, R., J. Box, C. Miege, E. Burgess, J. McConnell (2012), Measurements of snow accumulation rates and depth to the perennial firn aquifer in south east Greenland from the Arctic Circle Traverse 2010 and 2011, paper presented at 45th AGU Fall Meeting, San Francisco, Abstract C13G-07.

Gardner, A.S. and M. Sharp (2007), Influence of the Arctic Circumpolar Vortex on the Mass Balance of Canadian high Arctic Glaciers. *J. Climate*, 20, 4586–4598.

Gardner, A.S., G. Moholdt, B. Wouters, G. J. Wolken, D. O. Burgess, M. Sharp, J. G. Cogley, C. Braun, and C. Labine. (2011), Sharply increased mass loss from glaciers and ice caps in the Canadian Arctic Archipelago, *Nature*, 473(7347), 357-360.

Gardner, A. S., G. Moholdt, J. G. Cogley, B. Wouters, A. A. Arendt, J. Wahr, E. Berthier, R. Hock, W. T. Pfeffer, G. Kaser, S. R. M. Ligtenberg, T. Bolch, M. J. Sharp, J. O. Hagen, M. R. van den Broeke & F. Paul (2013), A Reconciled Estimate of Glacier Contributions to Sea Level Rise: 2003 to 2009. *Science*, 340, 852-857.

Gascon, G., M. Sharp, and A. Bush (2013), Changes in the melt season characteristics on Devon Ice Cap, Canada, in the 21st century, and their association with the Arctic atmospheric circulation, *Ann. Glaciol.*, 54(63),101-110, doi: 10.3189/2013AoG63A601.

Harper, J., N. Humphrey, W. Pfeffer, J. Brown, and X. Fettweis (2012), Greenland contribution to sea level rise buffered by meltwater storage in firn, *Nature*, 491, 240-243.

Humphrey, N.F., J.T. Harper, and W.T. Pfeffer (2012), Thermal tracking of meltwater retention in Greenland's accumulation area, *J. Geophys. Res.*, 117, F01010, doi:10.1029/200JF002083.

Koerner, R. (1977), Devon Island Ice Cap: Core Stratigraphy and Paleoclimate. *Science*, 196 (4285), 15-18.

Koerner, R. (2005), Mass balance of glaciers in the Queen Elizabeth Islands, Nunavut, Canada. *Ann. of Glaciol*., 42(1) 417-423, doi: 10.3189/172756405781813122.

Kovacs, A, A. J. Gow, and R. M. Morey (1995), The in-situ dielectric constant of polar firn revisited, *Cold Reg. Sci. Technol.*, 23(3), 245–256.

Meehl, Gerald A., and Coauthors, 2012: Climate System Response to External Forcings and Climate Change Projections in CCSM4. *J. Climate*, 25, 3661–3683, doi: http://dx.doi.org/10.1175/JCLI-D-11-00240.1

Miège, C., R.R. Forster, J.E. Box, E.W. Burgess, J.R. McConnell, D.R. Pasteris, and V.B. Spikes (2013), Southeast Greenland high accumulation rates derived from firn cores and ground-penetrating radar, *Ann. Glaciol.*, 54(63), 322–332, doi:10.3189/2013AoG63A358.

Müller, F. (1962), Zonation in the accumulation area of the glaciers of Axel Heiberg Island, *J. Glaciol.*, 4(33), 302–313.

Pfeffer, W.T., M.F. Meier, and T.H. Illangasekare (1991), Retention of Greenland runoff by refreezing: Implications for projected future sea level change, *J. Geophys. Res.*, 96(C12), 22,117–22,124.

Pfeffer, W.T., and N.F. Humphrey (1996), Determination of timing and location of water movement and ice-layer formation by temperature measurements in sub-freezing snow. *J. Glaciol.*, 42(141), 292–304.

Pfeffer, W.T., and N.F. Humphrey (1998), Formation of ice layers by infiltration and refreezing of meltwater. *Ann. Glaciol.*, 26, 83–91.

Radić, V. and R. Hock (2011), Regionally differentiated contribution of mountain glaciers and ice caps to future sea-level rise. *Nature Geosci.*, 4(2), 91–94, doi: 10.1038/ngeo1052.

Reijmer C.H., M.R. Van den Broeke, X. Fettweis, J. Ettema, L.B.and Stap (2012), Refreezing on the Greenland ice sheet: a comparison of parameterizations. Cryosphere, 6(4), 743–762, doi: 10.5194/tc- 6-743-2012

Sharp, M., D. O. Burgess, J. G. Cogley, M. Ecclestone, C. Labine, and G. J. Wolken (2011), Extreme melt on Canada's Arctic ice caps in the 21st century, *Geophys. Res. Lett.*, 38, L11501, doi:10.1029/2011GL047381.

Sylvestre, T., L. Copland, L. Gray, M. N. Demuth, and M. Sharp (2013), Spatial patterns of snow accumulation across Belcher Glacier, Devon Ice Cap. *J. Glaciol.*, 59(217), 874-882, doi: 013JoG12J227.

van Wychen W., L. Copland, L. Gray, D. Burgess, B. Danielson, and M. Sharp (2012), Spatial and temporal variation of ice motion and ice flux from Devon Ice Cap, Nunavut, Canada. *J. Glaciol.*, 58(210), 657–664, doi: 10.3189/2012JoG11J164.

Wolken, G., M. Sharp, L. and Wang (2009), Snow and ice facies variability and ice layer formation on Canadian Arctic ice caps, 1999-2005, *J. Geophys. Res.*, 114, F03011, doi:10.1029/2008JF001173.

Zdanowicz, C, A. Smetny-Sowa, D. Fisher, N. Schaffer, L. Copland, J. Eley, and F. Dupont (2012), Summer melt rates on Penny Ice Cap, Baffin Island: Past and recent trends and implications for regional climate, *J. Geophys. Res.*, 117, F02006 (doi:10.1029/2011JF002248).

Chapter 4

How well is firn densification represented by a physically-based multilayer model? Model evaluation for the Devon Ice Cap, Nunavut, Canada[3]

4.1 Introduction

Mass loss from polar ice sheets and ice caps contributes significantly to eustatic sea level rise, and has been increasing since the beginning of the 21st century [e.g. *Sharp et al.*, 2011; *Gardner et al.*, 2011, 2013; *Svendsen et al.*, 2013]. Meltwater storage in firn (compacted snow that has survived at least once melt season) through refreezing and retention currently limits the amount of surface melt from polar ice sheets and ice caps that reaches the oceans [*Harper et al.*, 2012]. Meltwater can infiltrate firn by either homogeneous or heterogeneous percolation. Homogeneous percolation consists of uniform vertical flow of meltwater, while heterogeneous percolation involves vertical flow of meltwater concentrated in specific areas, typically referred to as piping [e.g.: *Pfeffer et al.*, 1991]. Meltwater storage in firn by refreezing is most significant in the percolation zone of the accumulation area [e.g.: *van Pelt et al.*, 2013], where heterogeneous percolation dominates [e.g.: *Pfeffer et al.*, 1991; *Humphrey et al.*, 2012] (Figure 4-1).

A projected increase in Arctic air temperatures of at least 2 ˚C over the next 20 years [*Meehl et al.*, 2012] will initially increase the amount of percolating meltwater that refreezes in the shallow subsurface layer of ice caps. Such changes could raise the near surface temperature of the ice caps through latent heat release and significantly increase rates of firn densification [*Zdanowicz et al.*, 2012, *Bezeau et al.*, 2013]. Warming of the firn could promote further surface melt and

[3] A version of this chapter was submitted to *Journal of Glaciology* as Gascon, G., M. Sharp, D. Burgess, P. Bezeau, A. Bush, S. Morin, and M. Lafaysse, How well is firn densification represented by a physically-based multilayer model? Model evaluation for the Devon Ice Cap, Nunavut, Canada.

thus internal refreezing. An increase in mean summer air temperature of approximately 4 ˚C was measured on the Devon Ice Cap, Nunavut, Canada, between 2004 and 2010 [*Gascon et al.*, 2013]. This warming was associated with the rapid densification of the first 4 m of firn below the surface of the accumulation area of the ice cap, and with migration of the upper boundaries of the different snow facies zones to higher elevations after 2005 [*Gascon et al.*, accepted]. This rapid densification occurred by heterogeneous refreezing of meltwater, and is progressively reducing the water storage potential and refreezing capacity of the firn layer of the ice cap. This will lead to an increase in the fraction of meltwater that runs off, enhancing mass loss from the ice cap.

Evaluation of how quickly this transition towards increasing surface runoff will occur requires accurate modeling of firn processes. Such processes are currently represented by parameterizations implemented in land surface models [e.g. *Vionnet et al.*, 2012] that are coupled with climate models [e.g. *Reijmer et al.*, 2012; *van Angelen et al.*, 2013]. In the absence of direct observations, refreezing parameterizations have been validated by comparing them against each other [*Reijmer et al.*, 2012]. Although that study showed that the six tested refreezing parameterizations agreed with each other (using the Regional Atmospheric Climate Model (RACMO2) as a benchmark), none of them accounted explicitly for heterogeneous percolation of meltwater. Without evaluation against observations, it is impossible to determine whether these parameterizations accurately represent the magnitude and distribution of refreezing. Since refreezing parameterizations are included in models that are being used to predict future glacier mass balance and sea level changes, it is critical to determine whether they are capable of simulating changes in firn processes that are as large and rapid as those that have been observed in the accumulation area of the Devon Ice Cap since 2005.

Here, we use the physically-based multilayer snowpack model Crocus to simulate changes in firn properties on the Devon Ice Cap during the period of rapid summer warming between 2004 and 2012. Model results are compared with the evolving firn stratigraphy recorded in 14 firn cores drilled at 4 sites in the accumulation zone of the ice cap over the study period (Figure 4-2).

4.2 Methods

4.2.1 Model description

We used the detailed 1D multilayer snowpack model Crocus [*Vionnet et al.*, 2012] that is currently implemented in SURFEX [*Salgado and Le Moigne*, 2010]. Crocus computed the energy and mass balance of the snowpack and accounts for surface melting, internal melting/refreezing, compaction, snow metamorphism, snow aging, and sublimation enhancement during snow drift. As the model domain was limited to the thickness of the firn layer, bottom melting was not activated in the simulations. Crocus vertically discretizes firn stratigraphy with up to 50 layers ranging in thickness from 0.05 m close to the surface to 10 m at depth. Each layer was characterized in terms of its initial density, liquid water content, temperature, thickness, and snow grain parameters (dendricity, sphericity, grain size, and age). Age of each of the layers was determined based on the rate of accumulation of ~0.23 m w.e. a^{-1} over the surveyed area of the Devon Ice Cap [*Colgan and Sharp*, 2008]. Given that rate, a thickness of 10 m w.e. represents 43.5 years of net accumulation. In the absence of direct observations of snow grain parameters, we tested the model using several dendricity, sphericity, and grain size values. As varying the snow grain parameters did not change the outcome of the simulations, we used the model's default parameter values to initialize the physical properties of snow layers. The number and thickness of layers vary in time during simulations to represent the evolution of snowpack characteristics resulting from all the processes accounted for in the model.

Vertical percolation of meltwater is gravitationally-driven, and the water flow solution procedure starts from the top layer and proceeds downward [*Vionnet et al.*, 2012]. Crocus assumes homogeneous infiltration of water into firn. Vertical percolation of surface meltwater through a given layer is allowed when its liquid water content exceeds its maximum liquid water holding capacity, assuming that the layer can no longer freeze liquid water. The model's default maximum liquid water holding capacity ($W_{\mathrm{liq\ max}}$) is expressed as 5 % of the total pore volume [*Vionnet et al.*, 2012]:

$$W_{liq\,\max} = 0.05\rho_w D\left(\rho_i - \frac{(\rho - LWC)}{\rho_i}\right) \tag{1}$$

where D is the snow layer thickness, LWC is the liquid water content, and ρ_w, ρ_i, and ρ are the water, ice and snow layer density, respectively. Under this parameterization, the model neglects the formation of capillary barrier such as thick impermeable ice layers. Instead, once an ice layer has reached its maximum liquid water holding capacity, the model forces meltwater to flow through it. A percentage of total pore volume smaller (larger) than 5% decreases (increases) liquid retention, which enhances (reduces) vertical percolation and refreezing of meltwater at depths. As Crocus is used primarily to simulate snowpacks that are warmer and moister than that which characterizes the Devon Ice Cap, the model was tested for maximum liquid water holding capacities ranging between 1 and 6 % of pore volume. A maximum liquid water holding capacity of 3 % led to the best model simulations over the Devon Ice Cap, and so the results presented here are from those simulations.

4.2.2 Initial conditions

Model runs were initialized using field observations for April 30, 2004 at Sites 1 and 2, and April 30, 2006 at HB 9-1 and HB 13-7 (Figure 4-2). Simulations ran continuously at a time step of 15 minutes until May 1st 2012 for all sites. Initial density profiles were derived from 15-m firn cores drilled in 2004 at Sites 1 and 2, and from 4.5-m cores drilled in 2006 at HB 9-1 and HB 13-7. Detailed analyses of these cores are presented in *Bezeau et al.* [2013]. Density profiles were derived by dividing the mass of each core segment by its volume. Core segments were 0.04-0.25 m in length, and consisted of the relatively homogeneous material between density transitions along the core. Average density measurement error is estimated to be 40 kg m^{-3}. Initial density profiles below 5 m at HB 9-1 and HB 13-7 were set to 550 kg m^{-3} to 25-m depth based on firn density profiles in the upper-percolation area of the Greenland Ice Sheet [*Brown et al.*, 2012]. Initial density profiles were also extended to a depth of 25-m at Sites 1 and 2 with an initial density of 550 kg m^{-3}. The inclusion of deeper layers was evaluated, but did not change the outcome of the simulations.

In the absence of detailed firn temperature profiles for 2004, 16-day average spring 2012 firn temperature measurements were used to represent the end of winter temperature profiles. These were made with 10 kΩ negative temperature coefficient thermistors (accuracy ± 0.1°C) located every 1 m to a depth of 15 m at Site 1 and Site 2, and at 10 and 15 m depth at HB 9-1 and HB 13-7 (see *Bezeau et al.*, [2013] for details). At HB 9-1 and HB 13-7, spring 2012 firn temperature measurements were only available for 10 and 15 m below the snow surface. At these two sites, vertical firn temperature profiles were extrapolated between the surface and 10 m below the surface assuming the same vertical temperature gradients as those derived from temperature measurements at Site 1 and Site 2. At all sites, we assumed a constant firn temperature below 15 m. One 24-h average firn temperature measurement made at 10 m below the snow surface at Site 1 in 2004 allowed us to determine the error associated with our chosen temperature profiles. Between 2004 and 2012, the firn temperature at 10-m depth at Site 1 increased by 3.8 °C, from -21.3 to -17.5 °C. Even so, firn temperatures are well below the melting point of ice and firn. We tested the model with cooler firn temperatures at Site 1, but this did not change the outcome of the simulations. Therefore, we assumed that using the 2012 firn temperature profiles at all sites would not significantly alter the firn density profile evolution during the simulations.

4.2.3 Atmospheric forcing

Crocus requires inputs of air temperature, specific humidity, wind speed, short-wave and long-wave radiation, precipitation rate, and atmospheric pressure.

Three-hourly surface data from the North American Regional Reanalysis (NARR) [*Mesinger et al.*, 2006] were used to force the model between 2004 and 2012. Local observations of wind and air temperature from automated stations at Site 1 and Site 2 between 2004 and 2010, and shortwave and longwave radiation budgets from a net radiometer at Site 2 between 2007 and 2010 were used to validate and adjust NARR fields prior to using them to drive simulations. Details of meteorological field data collection are provided in *Gascon et al.* [2013]. NARR temperature fields were downscaled from Site 1 to HB 9-1, and Site 2 to HB 13-7, using an environmental lapse rate of 4.9 °C km^{-1} [*Gardner et al.*, 2009]. Under conditions of flat and uniform topography, the wind field and the incoming shortwave radiation histories were assumed to be uniform between sites. The evolving albedo, surface fluxes and surface energy balance were calculated by the model at each site. Annual end-of-winter snowpack depth and density measurements from snow pits [*Bezeau et al.*, 2013] were used to adjust NARR precipitation values at all four sites. Based on linear scaling between NARR precipitation and field observations, we found that NARR underestimated precipitation between 30 and 50%. Simulations presented in this paper were performed with consideration of the removal of potential biases due to precipitation errors.

4.2.4 Data for Model Comparison

Modeled density profiles, and mass and thickness changes between 2004 and 2012 were compared to field observations. Model density profiles were compared with measured profiles from 4.5-m cores drilled in 2008 and 2011 (Site 1, HB 9-1, and HB 13-7), and from 15-m firn cores drilled in 2012 (all sites). Detailed descriptions of these cores are provided in *Bezeau et al.* [2013]. The masses of firn and ice in each core were calculated by multiplying each layer's thickness by its density, and summing the products down to 4.5 or 15 m depth. Both modeled and observed density profiles were linearly extrapolated to uniform thickness layers of 0.05 m to facilitate comparison. The percent difference, root mean square error, and mean error were used to assess the differences between modeled and observed masses for the profiles as a whole (Table 4-1).

4.3. Model evaluation

Crocus performed relatively well at all sites, as seen from modeled density profiles at the end of the simulation period relative to observations (Figure 4-3). The evolution of density profiles throughout the simulations however suggests that Crocus overestimated firn densities in the upper part of the profile, with larger overestimations at higher-elevation sites (Figure 4-4). The observed difference in density profiles were quantified by the difference between modeled and observed mass of the firn columns. The mass percent difference between model and observations for the upper 15 m of the firn for the period 2004-2012 ranged from -2 % at HB 9-1, to 16 % at Site 1. Across all sites, the 2012 simulations overestimated the mass of the upper 4.5 m of the firn (including winter snowpack) by an average of 15 % relative to observations, but they underestimated the mass of the lower part of the firn column (4.5-15 m) by 5 %. The modeled mass of the upper 4.5 m of the firn was also an overestimate relative to observations at all sites in all years.

Modeled and observed winter snowpacks mass were first compared to determine whether differences between the modeled and observed winter snowpack alone could account for the differences in modeled and observed masses of firn. The average percent difference between modeled and observed winter snowpack mass ranged between 3 and 5%, with an average of 4 % (Table 4-2). Although NARR atmospheric forcing data were validated and adjusted with ground observations, the 3-hourly resolution of these data was still coarse, and could have accounted for the difference in snowpack mass between model and observations. A larger modeled winter snowpack implies that more mass was initially added to the firn column in the model than was the case in reality, and this contributes to the model overestimation of firn mass. Crocus's average 4% overestimation of the winter snowpack mass relative to observations is, however, smaller than its 10% average overestimation of the mass of the entire column of firn (Table 4-3). This suggests that the differences between modeled and observed mass and density profiles over the course of the simulation are due to a combination of the model's overestimation of winter snowpack and its parameterization of firn processes.

In Crocus, water initially froze closer to the surface than in observations, creating a positive model density bias near the surface, and a negative density bias at depth. The assumption of homogeneous percolation implies that the capacity for refreezing meltwater in firn is a function of the total pore volume of the firn layer. In reality, percolation is heterogeneous, which allows localized deep infiltration of surface melt and the formation of discontinuous ice layers (Figure 4-1a). In the accumulation area, deposition of new snow over each winter added new pore volume surrounded by a matrix of snow crystals. This most likely acted as a sink for percolating meltwater at the start of the following melt season. As Crocus modeled percolation as a homogeneous process, this created conditions that favored near surface freezing. Thus, modeling percolation as homogeneous, and as such, not considering deep heterogeneous percolation, resulted in too much mass being retained in the upper part of the firn profile relative to observations, and in insufficient mass accumulating at depths (Figure 4-4c-d). Improved model performance at lower-elevation sites relative to higher-elevation sites (Figure 4-3) may suggest that homogeneous percolation is a more realistic assumption at sites where air temperature is warmer and more surface melt is generated.

In addition, Crocus density profiles at all sites showed less vertical variability below 4.5 m depth than observed density profiles (Figure 4-3). The presence of alternating layers of firn and ice below 5 m is evident in observed density profiles and firn cores (Figure 4-5), but is not seen in the modeled density profiles. Crocus allows vertical percolation of surface meltwater through a given layer only when it becomes saturated and can no longer freeze liquid water. Under year-round sub-zero firn temperatures conditions, this implies that water-saturated layers would freeze during and/or at the end of the summer, automatically forming ice layers. At the same time, Equation 1 implies that when an ice layer forms, its liquid water holding capacity is very small, and water is forced to percolate through the ice layer rather than pond or flow laterally above it. This, combined with the representation of deep heterogeneous percolation as a homogeneous process, makes it impossible to simulate the survival of residual firn bodies between ice layers.

4.4 Implications for mass balance modeling

A vertical distribution of refreezing in the firn that is different from what is observed may be simulated when snowpack models are run for climate-warming scenarios. In our simulations, large amounts of meltwater refroze homogeneously close to the surface whereas, in reality, part of the surface meltwater appears to have percolated to greater depths by heterogeneous percolation. Observations show that heterogeneous percolation can lead to the vertical transport of meltwater via saturated pipes to depths of at least 10 m in Greenland [*Humphrey et al.*, 2012], and similar piping signatures have been observed on the Devon Ice Cap (Figure 4-1). Under a rapid climate warming scenario, melt can potentially spread quickly to large areas where it was previously very limited or non-existent. As a result, the upper boundaries of the wet snow and percolation zones may migrate rapidly to higher elevations. This has been observed on the Devon Ice Cap since 2005 [*Bezeau et al.*, 2013; *Gascon et al., 2013*]. Similar migration of the snow facies on the Greenland Ice Sheet may be observed in the near-future since recent extreme melt events [*Nghiem et al.*, 2012; *Hall et al.*, 2013] suggest that the dry snow zone there may disappear within the next decade [*McGrath et al.*, 2013]. Without consideration of heterogeneous percolation, however, models could overestimate refreezing near the surface, leading to an overestimation of the representation of the migration of the different snow facies to higher elevations. As the migration of snow facies to higher elevations is associated with a reduction of pore space in firn, and will ultimately lead to an increase in surface runoff, Crocus's current refreezing parameterizations may lead to an overestimation of surface runoff because they result in too much ice accumulating close to the surface.

Crocus' current parameterizations of ice layers may, however, have the opposite effect on the representation of surface runoff. Until recently, thick impermeable ice layers had not been observed in any ice sheet or ice cap, making it impossible to know whether or how meltwater might percolate through them. *Gascon et al*. [accepted] showed that the presence of thick ice layers on the Devon Ice Cap reduces pore space in firn and can enhance surface runoff and the amount of refreezing of meltwater. Crocus, however, allows meltwater to percolate through ice layers and refreeze evenly in the firn below. By allowing water to percolate through ice layers, the model limits horizontal runoff from the overlying firn and snowpack. This forces percolation to greater depths than percolating water can reach in reality. This would artificially slow down runoff response to summer warming and hence, underestimate the sea-level rise contribution from ice sheets and ice caps in response to climate warming.

4.5 Conclusion

We used a combination of data from firn cores and from NARR to force simulations with the Crocus snowpack model for the Devon Ice Cap, Nunavut during the period 2004 to 2012. We compared model simulations with the evolving firn stratigraphy recorded in 14 cores drilled at 4 elevations in the accumulation zone of the Devon Ice Cap over that same period. Crocus performs relatively well at all sites, with modeled mass bias in the upper 15 m of the firn ranging between -2 and +16% relative to observations. Inspection of the differences between modeled and observed density profiles showed that Crocus overestimated the mass of the top 4.5 m of firn and ice at all sites, but underestimated it below 4.5 m. Annual winter snow accumulation continually added new pore volume close to the surface. As Crocus represents heterogeneous percolation as a homogeneous process, this created conditions that favoured near surface freezing and insufficient refreezing at depths. In addition, Crocus's current parameterization of ice layers forced meltwater to percolate through them, preventing the buildup of thick impermeable ice layers. Given that percolation in the upper part of the accumulation area of ice caps and ice sheets tends to be heterogeneous rather than homogeneous, and given the potential importance of thick ice layers in restricting vertical meltwater drainage, it is important for models to simulate i) both heterogeneous and homogeneous percolation, and ii) the quasi-impermeability of ice layers to meltwater flow in order to accurately reproduce firn density profile evolution and mass balance through periods of climate warming.

Tables

Table 4-1: Comparative statistics between modeled and observed mass (kg m^{-2}).

	Site 1		HB 9-1		HB 13-7		Site 2	
	RMSE	ME	RMSE	ME	RMSE	ME	RMSE	ME
2008	176	87	94	17	142	55	---	---
2011	191	145	187	108	157	31	---	---
2012	221	154	176	89	127	47	91.3	53.1
2012 (15 m)	148	82	123	-11	118	29	138.5	107.1

Table 4-2: Percent difference between modeled and observed winter Snowpack mass (kg m^{-2}).

Site	4.5-m depth			15-m depth
	2008	2011	2012	2012
Site 1	128*	-9	12	12
HB 9-1	5	15	0	0
HB 13-7	5	2	0	0
Site 2	---	---	5	5
Average	5	3	4	4

*: Simulation forced with three times the observed snowpack to obtain realistic results. This result was ignored in the average.

Table 4-3: Percent difference between modeled and observed mass.

Site	4.5-m depth			15-m depth	4.5-15 m depth
	2008	2011	2012	2012	2012
Site 1	19	29	33	16	-10
HB 9-1	3	21	15	-2	9
HB 13-7	9	13	6	4	-3
Site 2	---	---	7	13	-16
Average	10	21	15	8	-5

Overall average: 10%

Figures

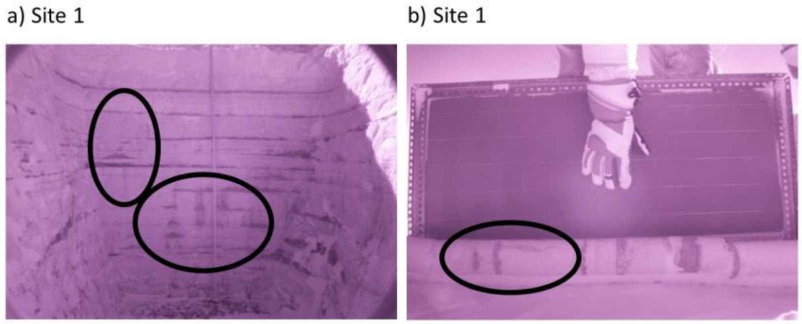

Figure 4-1: Examples of heterogeneous percolation and refreezing for a) the top 3 m below the surface at Site 1 in 2011, and b) at 8-9 m depth at Site 1 in 2011. Photos are infrared photography using a modified Fuji FinePix S9000 digital camera and an infrared filter of 850 nm.

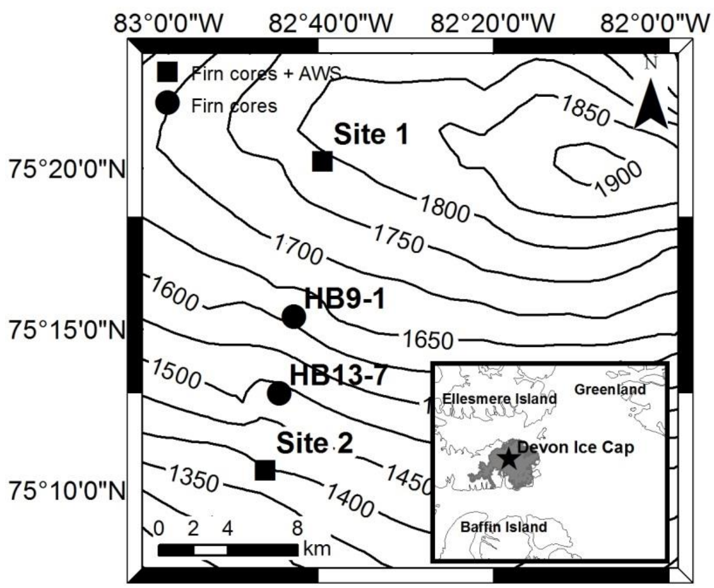

Figure 4-2: Map of the Devon field sites: Site1 (1800 m a.sl.), HB 9-1 (1610 m a.s.l.), HB 13-7 (1490 m a.s.l.), and Site 2 (1400 m a.s.l.). In 2004, Site 1 and HB 9-1 were both located in the percolation zone of the Devon Ice Cap, while HB 13-7 and Site 2 were located in the wet snow zone. By 2012, Site 1 was still located in the percolation zone, while HB 9-1 was in wet snow zone, and HB 13-7 and Site 2, in the superimposed ice zone. Squares denote locations of weather stations, net radiometers, and firn core sites, and circles denote locations of firn core sites.

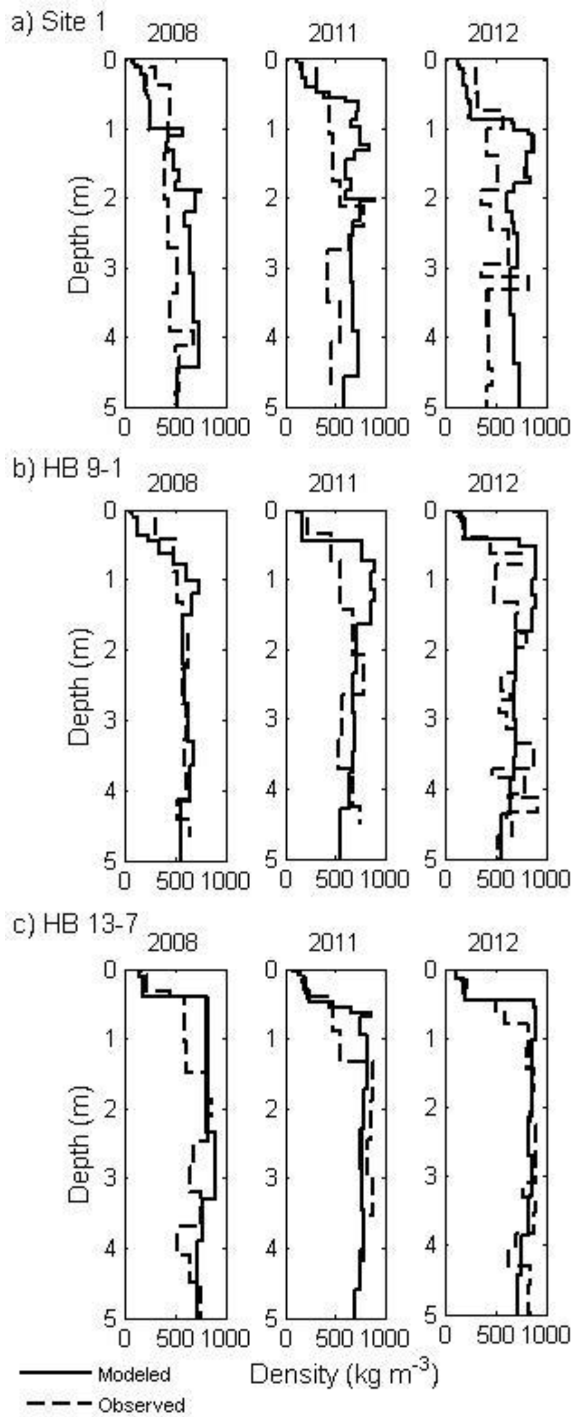

Figure 4-3: Modeled (solid) and observed (dash) density profile (kg m^{-3}) of the top 5 m of firn for 2008, 2011 and 2012 at a) Site 1, b) HB 9-1, and c) HB 13-7. Maximum water content capacity of 3 % is used.

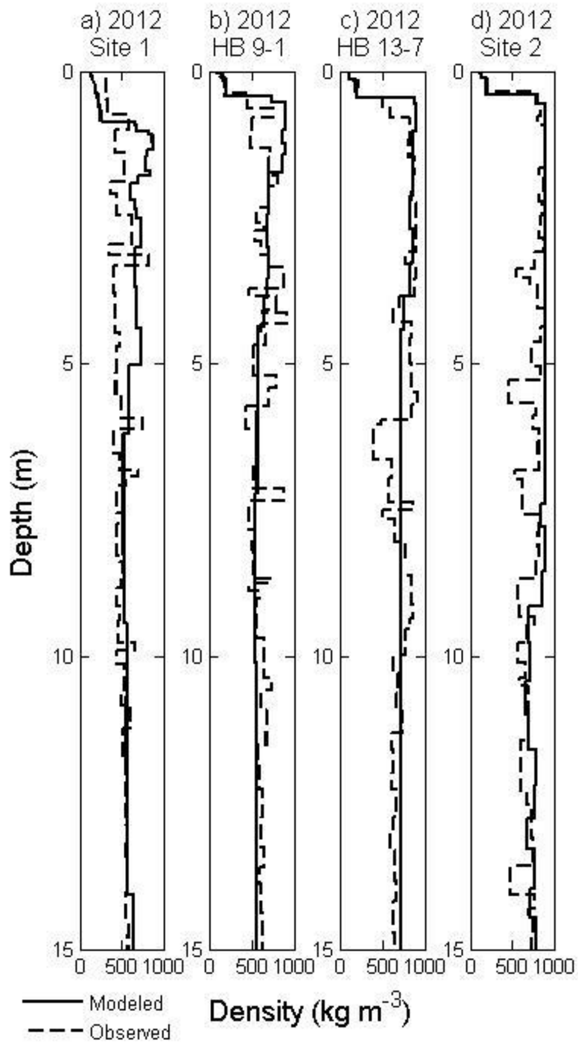

Figure 4-4: Modeled (solid) and observed (dash) density profile (kg m^{-3}) of the top 15 m of firn for 2012 at a) Site 1, b) HB 9-1, c) HB 13-7, d) Site 2. Maximum water content capacity of 3 % is used.

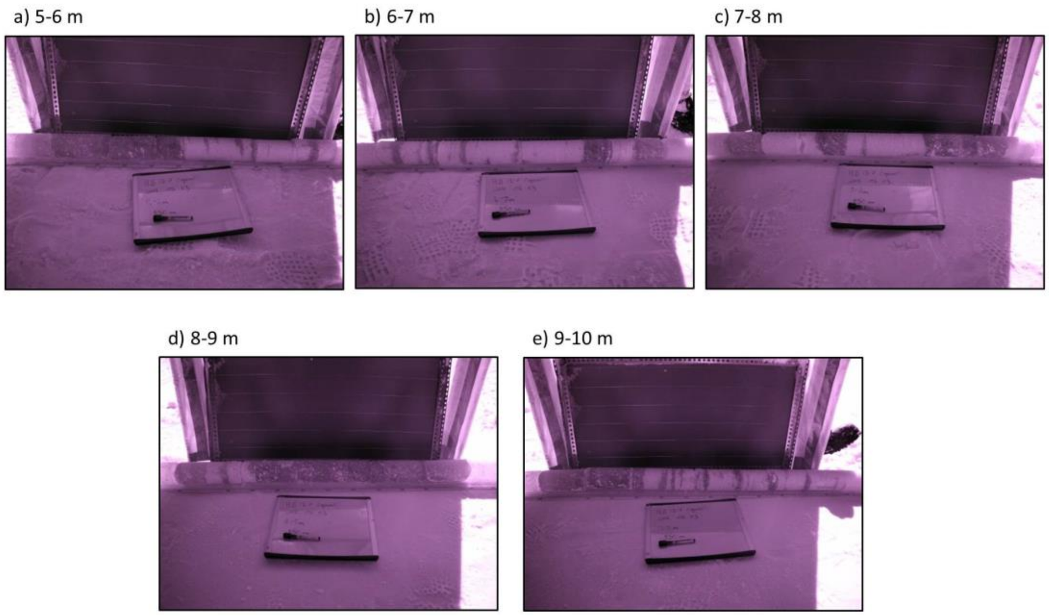

Figure 4-5: Firn stratigraphy showing alternating firn and ice layers between 5 and 10 m depth at HB 13-7 in spring 2012. Photos are infrared photography using a modified Fuji FinePix S9000 digital camera and an infrared filter of 850 nm.

4.6 References

Bezeau, P., M. Sharp, D. Burgess, and G. Gascon (2013), Firn profile changes in response to extreme 21st century melting at Devon Ice Cap, Nunavut, Canada, *J. Glaciol.*, 59(217), 981-991, doi:10.3189/2013JoG12J208.

Brown, J., J. Bradford, J. Harper, W.T. Pfeffer, N. Humphrey, and E. Mosley-Thompson (2012), Georadar-derived estimates of firn density in the percolation zone, western Greenland ice sheet, *J. Geophys. Res.*, 117, F01011, doi:10.1029/2011JF002089.

De Jong, J.T. (2013), Recent Changes in Glacier Facies Zonation on Devon Ice Cap, Nunavut, Detected from SAR Imagery and Field Validation Methods, M.Sc. thesis, Dep. of Phys.Geog., University of Ottawa, Ottawa, Ontario, Canada.

Gardner, A.S., M.J. Sharp, R.M. Koerner, C. Labine, S. Boon, S.J. Marshall, D.O. Burgess, and D. Lewis (2009), Near-Surface Temperature Lapse Rates over Arctic Glaciers and Their Implications for Temperature Downscaling. *J. Climate*, 22, 4281–4298. doi: http://dx.doi.org/10.1175/2009JCLI2845.1

Gardner, A.S., G. Moholdt, B. Wouters, G.J. Wolken, D.O. Burgess, M. Sharp, J.G. Cogley, C. Braun, and C. Labine (2011), Sharply increased mass loss from glaciers and ice caps in the Canadian Arctic Archipelago, *Nature*, 473(7347), 357-360.

Gardner, A.S., G. Moholdt, J.G. Cogley, B. Wouters, A.A. Arendt, J. Wahr, E. Berthier, R. Hock, W.T. Pfeffer, G. Kaser, S.R.M. Ligtenberg, T. Bolch, M.J. Sharp, J.O. Hagen, M.R. van den Broeke, and F. Paul (2013), A Reconciled Estimate of Glacier Contributions to Sea Level Rise: 2003 to 2009. *Science*, 340, 852-857.

Gascon, G., M. Sharp, and A.G. Bush (2013), Changes in the melt season characteristics on Devon Ice Cap, Canada, in the 21st century, and their association with the Arctic atmospheric circulation, *Ann. Glaciol.*, 54(63):101-110, doi: 10.3189/2013AoG63A601.

Gascon, G., Sharp, M.J., Burgess, D., and Bezeau, P. (accepted), Changes in accumulation-area firn stratigraphy and meltwater flow during a period of climate warming: Devon Ice Cap, Nunavut, Canada, *J. Geophy. Res.*, doi: 10.1002-2013JF002838.

Hall, D. K., J. C. Comiso, N. E. DiGirolamo, C. A. Shuman, J. E. Box, and L. S. Koenig (2013), Variability in the surface temperature and melt extent of the Greenland ice sheet from MODIS, *Geophys. Res. Lett.*, 40, 2114–2120, doi:10.1002/grl.50240.

Harper, J., N. Humphrey, W. Pfeffer, J. Brown, and X. Fettweis (2012), Greenland contribution to sea level rise buffered by meltwater storage in firn, *Nature*, 491, 240-243.

Humphrey, N.F., J.T. Harper, and W.T. Pfeffer (2012), Thermal tracking of meltwater retention in Greenland's accumulation area, *J. Geophys. Res.*, 117, F01010, doi:10.1029/200JF002083.

McGrath, D., W. Colgan, N. Bayou, A. Muto, and K. Steffen (2013), Recent warming at Summit, Greenland: Global context and implications, *Geophys. Res. Lett.*, 40, 2091–2096, doi:10.1002/grl.50456.

Mesinger, F., and Coauthors. 2006. North American Regional Reanalysis. *Bull. Amer. Meteor. Soc.*, 87, 343–360. doi: http://dx.doi.org/10.1175/BAMS-87-3-343.

Nghiem, S. V., D. K. Hall, T. L. Mote, M. Tedesco, M. R. Albert, K. Keegan, C. A. Shuman, N. E. DiGirolamo, and G. Neumann (2012), The extreme melt across the Greenland ice sheet in 2012, *Geophys. Res. Lett.*, 39, L20502, doi:10.1029/2012GL053611.

Pfeffer, W. T., M. F. Meier, and T. H. Illangasekare (1991), Retention of Greenland runoff by refreezing: Implications for projected future sea level change, *J. Geophys. Res.*, 96(C12), 22,117–22,124.

Reijmer C.H., M.R. Van den Broeke, X. Fettweis, J. Ettema, and L.B. Stap (2012), Refreezing on the Greenland ice sheet: a comparison of parameterizations, *Cryosphere*, 6(4), 743–762, doi: 10.5194/tc- 6-743-2012.

Salgado, R. and P. Le Moigne (2010), Coupling of the FLake model to the Surfex externalized surface model, *Boreal Environ. Res.*, 15, 231–244.

Sharp, M., D.O. Burgess, J.G. Cogley, M. Ecclestone, C. Labine, and G.J. Wolken (2011), Extreme melt on Canada's Arctic ice caps in the 21st century, *Geophys. Res. Lett.*, 38, L11501, doi:10.1029/2011GL047381.

Svendsen, P.L., O.B. Andersen, and A.A. Nielsen (2013), Acceleration of the Greenland ice sheet mass loss as observed by GRACE: Confidence and sensitivity, *Earth Planet. Sc. Lett.*, 364, 24-29, doi:/10.1016/j.epsl.2012.12.010.

van Angelen, J.H., J.T.M. Lenaerts, M.R. van den Broeke, X. Fettweis, and E. van Meijgaard (2013), Rapid loss of firn pore space accelerates 21st century Greenland mass loss, *Geophys. Res. Lett.*, 40, doi:10.1002/grl.50490.

van Pelt, W.J.J, J. Oerlemans, C.H. Reijmer, V.A. Pohjola, R. Pettersson, and J.H. Van Angelen (2012), Simulating melt, runoff and refreezing on Nordenskio¨ldbreen, Svalbard, using a coupled snow and energy balance model, *Cryosphere*, 6(3), 641–659m doi: 10.5194/tc-6- 641-2012

Vionnet, V., E. Brun, S. Morin, A. Boone, S. Faroux, P. Le Moigne, E. Martin, and J.-M. Willemet (2012), The detailed snowpack scheme Crocus and its implementation in SURFEX v7.2, *Geosci. Model Dev.*, 5, 773-791, doi :10.5194/gmd-5-773-2012.

Zdanowicz, C, A. Smetny-Sowa, D. Fisher, N. Schaffer, L. Copland, J. Eley, and F. Dupont (2012), Summer melt rates on Penny Ice Cap, Baffin Island: Past and recent trends and implications for regional climate, *J. Geophys. Res.*, 117, F02006 (doi:10.1029/2011JF002248).

Chapter 5
Conclusion

5.1 Summary

Results presented in this thesis combined the analysis of ground-based meteorological and geophysical measurements, climate re-analysis data, and an evaluation of the numerical snowpack model Crocus to investigate ice-climate interactions during a recent period of rapid warming of summer climate (from 2004 to 2012), and the impact of warming on the hydrology and stratigraphy of the firn layer of the Devon Ice Cap, Nunavut.

Using surface meteorological measurements for June-August during the period 2004 to 2010, we found that the length of the summer melt season increased at rates of 3.4 ($p<0.1$; weak significance), 6.1 ($p<0.01$) and 8.8 ($p<0.05$) days yr^{-1} at elevations of 1800, 1400 and 1000 m a.s.l. on the Devon Ice Cap respectively. Over that same period, the timing of melt onset advanced by 0.3, 4.4 ($p<0.01$) and 4.5 days yr^{-1} at 1800, 1400 and 1000 m a.s.l., respectively, for an average of 3 days yr^{-1} (non-significant). Similarly, the timing of freeze-up was delayed by 6.7, 5.4 ($p<0.05$) and 4.5 ($p<0.05$) days yr^{-1} at 1800, 1400 and 1000 m a.s.l., respectively, for a three-site average of 5.5 days yr^{-1}($p<0.05$). These large increase/decrease rates are, in part, the result of a cold 2004 summer, and extremely warm 2010 summer. As a result of the increasingly longer melt seasons, the calculated surface melt rate at 1400 m a.s.l. increased from 0.74 to 1.33 m w.e. yr^{-1} between 2007 and 2010. These changes are linked to two types of change in the Arctic atmospheric circulation: i) strengthening of the 500 hPa ridge over the Arctic in June-July, which resulted in increases in both the advection of warm air into the region and the occurrence of cloud-free conditions over the ice cap, causing the available melt energy to increase by 4-24% relative to periods in the June-July 2007-2010 epoch when a 500 hPa ridge was not developed, and ii) more frequent south-westerly low-pressure systems in August after 2004, which accounted for a 12-38% increase in available melt energy relative to the 2007-2010 August daily mean for periods that were storm-free. These stormy periods in August were associated with increases in both advection of warm air into the Arctic and net longwave radiation.

To document climate-driven changes in stratigraphy and meltwater flow within the firn layer of the Devon Ice Cap, Nunavut, 500 MHz ground-penetrating radar (GPR) surveys were conducted along a 40 km transect in each spring from 2007 to 2012. These surveys were supplemented by four 190 m by 100 m GPR grid surveys and analysis of 36 firn cores. Increased meltwater percolation and infiltration ice formation associated with higher surface melt rates modified the firn stratigraphy substantially over a horizontal distance of nearly 30 km. The most dramatic change involved the growth of a thick ice layer within the firn body. This layer grew primarily by upwards accretion over an initial widespread ice layer formed during summer 2005. It thickened by between 0.5 and 4.5 m over the study period, and filled much of the pore volume in the upper part of the firn, reducing both vertical percolation of meltwater into deeper sections of the firn and the water storage potential of much of the firn reservoir. Heterogeneous percolation of surface meltwater promoted by rolling topography played an important role in meltwater infiltration and drainage, encouraging rapid firn densification and lateral runoff within firn at the tops of wind-scoured and snow-deprived small hills, and ponding and refreezing of meltwater beneath surface depressions.

Finally, we compared simulations using the Crocus snowpack model with the evolving firn stratigraphy recorded in 14 cores drilled at 4 elevations in the accumulation zone of the Devon Ice Cap between 2004 and 2012 to determine whether snowpack models are able to accurately simulate changes in the firn stratigraphy as large and rapid as those observed. Simulations were forced with a combination of surface observations and climate reanalysis data. Crocus performs relatively well at all sites, with modeled mass difference in the upper 15 m of the firn ranging between -2 and +16% relative to observations. Crocus overestimated the mass of the top 4.5 m of firn at all sites, but underestimated it below 4.5 m. Annual winter snow accumulation continually added new pore volume close to the surface. As Crocus represents heterogeneous percolation as a homogeneous process, this created conditions that promoted excess near surface freezing and insufficient freezing at depths. In addition, Crocus's current parameterization of the permeability of ice layers forced meltwater to percolate through them, preventing the buildup of thick impermeable ice layers. Results thus highlighted the importance of incorporating heterogeneous percolation in firn, and of accurately representing the impermeability of ice layers to meltwater flow, in order to reproduce observed firn density profile evolution and mass balance through periods of climate warming.

5.2 Influence of atmospheric circulation

At the time when work on ice-atmosphere interactions on the Devon Ice Cap began (Chapter 2), the understanding of the relationship between changes in melt season characteristics on glaciers and ice caps in the Canadian Arctic and the atmospheric circulation was limited to increased melt under persistent July anticyclonic circulation [*Alt*, 1978, 1987; *Wang et al.*, 2005; *Sharp et al.*, 2011]. The study undertaken as part of this dissertation was the first to investigate the influence of atmospheric circulation on surface melt for the different months of the melt season separately. The work presented here demonstrated that strengthening of the 500 hPa ridge over the Arctic in June–July and more frequent southwesterly low-pressure systems in August after 2004 are both implicated in the observed increases in summer mean air temperature and surface energy balance that have led to increased surface melt on the Devon Ice Cap, Canada, between 2005 and 2010.

Since *Gascon et al.* [2013] was published, new work has shed additional light on the influence of changes in the atmospheric circulation on both the Greenland Ice Sheet and glaciers and ice caps in the Canadian Arctic. Studies extending to the end of the 2012 summer have shown that the summer atmospheric circulation pattern has been shifting towards more frequent and persistent anticyclonic circulation over Greenland and the Canadian Arctic since 2007 [*Fettweis et al.*, 2013; *Hanna et al.*, 2013; *Bezeau et al.*, 2013], especially in June [*Overland et al.*, 2012] This created a blocking high pressure feature which enhanced meridional flow across the Arctic and promoted warm air advection into the region [*Overland et al.*, 2012]. This atmospheric pattern was also associated with the record high surface melt extent on the Greenland Ice Sheet in July 2012 [*Hanna et al.*, 2013]. *Bezeau* [2013] investigated the relationship between Arctic summer atmospheric circulation and the surface mass balance of glaciers and ice caps in the Canadian Arctic Archipelago (CAA) between 1948 and 2012, and showed that the frequency of positive 500 hPa geopotential height anomalies was negatively correlated with glacier surface mass balance in the Canadian Arctic. Indeed, higher frequencies of positive 500 hPa geopotential height anomalies were observed prior to 1963 than from the mid-1960s to the mid-1990s. This was followed by a gradual rise in their frequency from the mid-1990s to the mid-2000s, prior to the sharp rise between 2007 and 2012 [*Bezeau*, 2013]. *Bezeau* [2013] found that the mean cumulative frequency of positive 500 hPa geopotential height anomalies over the CAA and western Greenland actually increased from 13.6% for 1948-2006 to 36.2% for 2007-2012; this increase corresponds to positive geopotential height anomalies occurring 2.7 times more often between 2007 and 2012 than during the 1948-2006 period over these regions.

It has been suggested that the observed shift in Arctic atmospheric circulation could have been caused by decreased Northern Hemisphere spring snow cover [*Overland et al.*, 2012] and/or decreased sea ice extent/volume in the Arctic, and particularly in the Chukchi Sea and off Siberia [*Francis and Vavrus*, 2012]. The total Arctic sea ice extent declined by 13% per decade in September from 1979 to

2012, and by 5% in April and May, and the sea ice volume decreased by 28% in September, 23% in April and 25% in May, over that same period, with recent extreme lows in 2007 and 2012 [*Bezeau, 2013*]. *Bezeau* [2013] also suggested that the combination of strong meridional heat advection in June, a decrease in sea ice volume/thickness during the summer, and the sea ice-albedo feedback all contributed to the development of persistent anticyclonic circulation over the Arctic in summer since June 2007.

These recent studies provide insights into the potential mechanisms responsible for the increase in melt season duration and surface melt observed on the Devon Ice Cap (Chapter 2, *Gascon et al.,* [2013]). *Bezeau* [2013] showed that stronger meridional heat advection in June was linked to an increase in the eddy heat flux at 500 hPa that drives the surface circulation. This atmospheric mechanism likely contributed to the observed advance of the timing of melt onset by an average of 3 days yr^{-1} on the Devon Ice Cap between 2004 and 2010 [*Gascon et al.*, 2013]. A decrease in sea ice volume and extent in the 21^{st} century [*Francis and Vavrus*, 2012; *Bezeau et al., 2*013] resulted in increased open water in the Arctic in summer after 2007, which potentially increased the vertical latent and heat fluxes from the ocean to the atmosphere, and, in turn, raised air temperature and geopotential height. According to the National Snow and Ice Data Center and the Pan-Arctic Ice Ocean Modeling and Assimilation System (http://psc.apl.washington.edu/wordpress/research/projects/arctic-sea-ice-volumeanomaly/), sea ice extent and volume reach their minima at the end of the melt season. It is possible that the additional latent heat flux from the ocean to the atmosphere at the end of the melt season provided enough upper-level support for mid-latitude cyclones to penetrate the Canadian Arctic region, and contributed to the freeze-up delay of an average of 5.5 days yr^{-1} on the Devon Ice Cap between 2004 and 2010 [*Gascon et al.*, 2013].

These changes in the Arctic atmospheric circulation may thus have triggered ice-climate interactions promoting surface melt, which resulted in the advance of the timing of melt onset and the delay in freeze up, and caused the surface melt rate at 1400 m a.s.l. to increase from 0.74 to 1.33 m w.e. yr^{-1} between 2007 and 2010.

5.3 Firn stratigraphy

Work reported in Chapter 3 was motivated by the results of Chapter 2. The increase in surface melt on the Devon Ice Cap between 2007 and 2010 raised questions about where and how the meltwater produced at high elevations flowed within the firn layer, and about where and how much of that water refroze. *Bezeau et al.* [2013] showed that the density of the top 2.5 m w.e. of the firn column on the Devon Ice Cap increased by 13-80% between 2004 and 2012 as a result of the formation of thick ice layers close to the surface. Building on their work, Chapter 3 (and *Gascon et al.* [accepted]) addressed how the thick ice layers observed actually grew, and how their growth interacted with the flow and storage of water within the firn layer by analyzing spatially continuous annual GPR surveys conducted in spring between 2007 and 2012. These surveys clearly showed that the rapid densification of firn observed on the Devon Ice Cap between 2007 and 2012 was caused by upward vertical accretion of ice above a thick quasi-impermeable ice layer that formed in the warm summer of 2005. Heterogeneous percolation of surface meltwater played a large role in the observed rapid firn densification. Refreezing was initially concentrated over small ridges, which eventually caused lateral flow diversion to basins, so that ponding and refreezing of meltwater in the concave regions occurred by spring 2011.

Meltwater refreezing and retention in firn currently delay the contribution of increasing melt to glacier runoff [*Harper et al.*, 2012]. However, mass loss from ice caps in the Arctic has been increasing since the late 20th century [e.g. Gardner and Sharp, 2007; *Sharp et al.*, 2011; *Gardner et al.*, 2011, 2013]. On the Devon Ice Cap, the ice layers significantly reduced vertical percolation of meltwater into deeper parts of the firn, to the point that water retention at 1400 m a.s.l. was ≤ 1% by 2010 [Chapter 3; *Gascon et al.*, accepted]. This reduction in the meltwater storage potential of the firn implies that the ability of firn on the Devon Ice Cap to buffer the relationship between surface melt and runoff through storage of water as ice within firn has already declined. Ultimately, this process has the potential to trigger a positive feedback at the ice-cap scale, whereby increasing amounts of near-surface runoff will occur from sections of the accumulation area where internal refreezing previously absorbed most or all of the annual melt, and thus reduce the surface mass balance of the ice cap.

The presence of numerous lakes in the accumulation area during the summer suggests a link between ice layer formation and the surface hydrology of the ice cap. *Wyatt* [2013] showed that lakes at high elevations, particularly in the wet-snow zone, either refreeze at the end of the melt season, or overflow at the surface through surface channels, and that the number of lakes that formed at higher elevations increased significantly between 1999 and 2011. As the formation of thick ice layers prevents deep drainage and facilitates surface ponding in summer, it is possible that the formation of ice layers in the shallow subsurface observed since 2005 [Chapter 3; *Gascon et al.*, 2013] may play a role in promoting increased formation of lakes in this region. These lakes, by freezing at the end of the summer, enhance ice layer formation, which, in turn, would facilitate lake formation in the following summer, creating a positive feedback enhancing both ice layer formation and the number and size of lakes. We believe that this feedback process is also implicated in the increased mass loss from the Devon Ice Cap and the CAA since 2005 [*Sharp et al.*, 2011; *Gardner et al*., 2011; 2013]

As the Devon Ice Cap's summit elevation is lower than that of the Greenland Ice Sheet summit, a faster response to climate warming is to be expected in both surface melt rates and firn stratigraphy. Nevertheless, a projected increase in Arctic air temperatures of up to 2 ˚C over the next 20 years [*Meehl et al.*, 2012] may lead to similar changes in firn stratigraphy on Greenland. Evaluation of how quickly the transition from meltwater percolating into firn to increasing surface runoff will occur is therefore critical to assessing future sea-level rise contributions from glaciers, ice caps and ice sheets in a period of climate warming. In order to achieve this, however, accurate modeling of firn processes is required. At the time the work presented in Chapter 4 was undertaken, snowpack models used for this purpose had yet to be evaluated against observations, so there was no way of knowing whether they were able to reproduce the extent and patterns of refreezing that have been observed in the accumulation area of the Devon Ice Cap since 2005. By evaluating the snowpack model Crocus, we found that the assumption of homogeneous percolation resulted in too much refreezing close to the surface. Despite this, the parameterization of permeability resulted in meltwater being allowed to percolate through thick ice layers and penetrate to greater depths within firn than it does in reality. This would have the consequence of artificially slowing down runoff response to summer warming and hence artificially delay the modeled sea-level rise contribution from ice sheets and ice caps that results from climate warming.

5.4 Concluding remarks and future work

Using a combination of NARR climate Re-analysis data, and ground-based weather station and net radiometer data, this thesis demonstrated that an increase in Arctic 500 hPa geopotential height in June and July, and an increase in frequency of low-pressure systems in the Canadian Arctic in August are associated with the observed increase in summer mean air temperature that has led to increased surface melt on the Devon Ice Cap since 2005 [*Gascon et al.*, 2013]. Using repeated GPR surveys and 36 firn cores, it was then shown that this increase in surface melt changed the firn stratigraphy on the Devon Ice Cap with the vertical accretion of a thick ice body within the upper 4m of the firn layer. This reduced the water storage potential of the ice cap, ultimately reducing the ability of firn to buffer the relationship between surface melt and runoff through storage of water as ice within firn [*Gascon et al.*, accepted]. Finally, Chapter 4 provided the first evaluation of a snowpack model against ground observations in a period of climate warming. The outcome of that model evaluation highlighted the importance of incorporating heterogeneous percolation in firn and of accurately representing the impermeability of ice layers to meltwater flow, in order to reproduce observed firn density profile evolution and mass balance through periods of climate warming.

Our observations of firn densification and melt water flow on the Devon Ice Cap suggest a need for surface mass balance models to incorporate more sophisticated treatments of percolation of meltwater and refreezing within firn than are currently available, and for the collection of long-term field datasets that would allow calibration and validation of those treatments.

In addition to improving the modelling of firn processes, outlook for future work includes the quantification of the amount of energy released to the atmosphere through latent and sensible heat fluxes from open water in the Arctic Ocean, and high resolution coupling between atmospheric and ocean models. The Nucleus for European Modelling of the Ocean has a high resolution domain over the Canadian Arctic [e.g. *Wang et al.*, 2012] and would be an ideal tool for future research, either as an offline tool to provide insights into the formation of new open water regions or, if fully coupled with an General Circulation Model (GCM), to further investigate ice-atmosphere-ocean feedbacks. The coupling of a snowpack/land model with a GCM would, in turn, allow better representation of the feedbacks between the atmospheric circulation, the surface albedo and firn processes. GCMs are however not yet capable of reproducing the observed change in frequency of summer anticyclonic atmospheric circulation patterns over the Arctic [*Bezeau,* 2013]. Improving the representation of the Arctic circulation in models is an essential step in research into ice-atmosphere interactions that has yet to be achieved. Until this happens, improving predictions of glacier mass balance in the Arctic will remain challenging.

5.5 References

Alt, B.T (1978), Synoptic Climate Controls of Mass-Balance Variations on Devon Island Ice Cap. *Arctic and Alpine Research*. 1, 61-80.

Alt, B.T. (1987), Developing synoptic analogues for extreme mass balance conditions on Queen Elizabeth Island ice caps. *J. Clim. Appl. Meteorol.*, 26, 1605– 1623.

Bezeau, P., M. Sharp, D. Burgess, and G. Gascon (2013), Firn profile changes in response to extreme 21st century melting at Devon Ice Cap, Nunavut, Canada, *J. Glaciol.*, 59(217), 981-991, doi:10.3189/2013JoG12J208.

Bezeau P. (2013), Variability in Summer Anticyclonic Activity over the Canadian Arctic Archipelago and west Greenland in the late 20th/early 21st centuries, and its impact on the firn stratigraphy of the Devon Ice Cap, M.Sc. thesis, Dep. of Earth and Atmospheric Sciences, University of Alberta, Edmonton, Alberta, Canada.

Fettweis, X., E. Hanna, C. Lang, A. Belleflamme, M. Erpicum, and H. Gallée (2013), Brief communication "Important role of the mid-tropospheric atmospheric circulation in the recent surface melt increase over the Greenland ice sheet", *The Cryosphere*, 7, 241-248, doi:10.5194/tc-7-241-2013.

Forster, R., J. Box, C. Miege, E. Burgess, J. McConnell (2012), Measurements of snow accumulation rates and depth to the perennial firn aquifer in south east Greenland from the Arctic Circle Traverse 2010 and 2011, paper presented at 45th AGU Fall Meeting, San Francisco, Abstract C13G-07.

Francis, J.A., and S.J. Vavrus (2012), Evidence linking arctic amplification to extreme weather in mid-latitudes, *Geophysical Research Letters*, *39*(6), doi: 10.1029/2012GL051000.

Gardner, A.S. et al. (2011), Sharply increased mass loss from glaciers and ice caps in the Canadian Arctic Archipelago, *Nature*, 473(7347), 357-360.

Gardner, A.S. et al. (2013), A Reconciled Estimate of Glacier Contributions to Sea Level Rise: 2003 to 2009, *Science*, 340, 852-857.

Gascon, G., M. Sharp, and A. Bush (2013), Changes in the melt season characteristics on Devon Ice Cap, Canada, in the 21st century, and their association with the Arctic atmospheric circulation, *Ann. Glaciol.*, 54(63),101-110, doi: 10.3189/2013AoG63A601.

Gascon, G., Sharp, M.J., Burgess, D., and Bezeau, P. (accepted), Changes in accumulation-area firn stratigraphy and meltwater flow during a period of climate warming: Devon Ice Cap, Nunavut, Canada, *J. Geophy. Res.*, doi: 10.1002-2013JF002838.

Hanna, E. et al. (2013), Atmospheric and oceanic climate forcing of the exceptional Greenland Ice Sheet surface melt in summer 2012, *Int. J. Climatol*, doi: 10.1002/joc.3743.

Harper, J., N. Humphrey, W. Pfeffer, J. Brown, and X. Fettweis (2012), Greenland contribution to sea level rise buffered by meltwater storage in firn, *Nature*, 491, 240-243.

Meehl, Gerald A., and Coauthors, (2012), Climate System Response to External Forcings and Climate Change Projections in CCSM4, *J. Climate*, 25, 3661–3683, doi: http://dx.doi.org/10.1175/JCLI-D-11-00240.1

Müller, F. (1962), Zonation in the accumulation area of the glaciers of Axel Heiberg Island, *J. Glaciol.*, 4(33), 302–313.

Pfeffer, W.T., M.F. Meier, and T.H. Illangasekare (1991), Retention of Greenland runoff by refreezing: Implications for projected future sea level change, *J. Geophys. Res.*, 96(C12), 22,117–22,124.

Overland, J. E., J.A. Francis, E. Hanna, and M.Wang (2012), The recent shift in early summer Arctic atmospheric circulation, *Geophysical Research Letters*, *39*(19).

Sharp, M., D.O. Burgess, J.G. Cogley, M. Ecclestone, C. Labine, and G.J. Wolken (2011), Extreme melt on Canada's Arctic ice caps in the 21st century, *Geophys. Res. Lett.*, 38, L11501, doi:10.1029/2011GL047381.

Wang, L., M.J. Sharp, B. Rivard, S. Marshall, and D. Burgess (2005), Melt season duration on Canadian Arctic ice caps, 2000–2004, *Geophys. Res. Lett.*, 32, L19502, doi:10.1029/2005GL023962.

Wang, Q., P.G. Myers, X. Hu and A.B.G. Bush (2012), Flow contraints on pathways through the Canadian Arctic Archipelago, *Atmosphere-Ocean*.

Wyatt, F. (2013), The spatial structure and temporal development of supraglacial drainage systems, and their influence on the flow dynamics of High Arctic ice caps, Ph.D. thesis, Dep. of Earth and Atmospheric Sciences, University of Alberta, Edmonton, Alberta, Canada.

van Angelen, J.H., J.T.M. Lenaerts, M.R. van den Broeke, X. Fettweis, and E. van Meijgaard (2013), Rapid loss of firn pore space accelerates 21st century Greenland mass loss, Geophys. Res. Lett., 40, doi:10.1002/grl.50490.